Chapter 3

Tests of Some Aspects of Spectral Averaging Theory in Large Shell Model Spaces for State, Spin-Cutoff and Occupancy Densities

3.1 Introduction

Extensions of the CLT results given in Chapter 2 to indefinitely large shell model spaces, enlarge the scope of spectral averaging theory as this will enable one to address problems in statistical nuclear physics, i.e. calculation of level densities and spin-cutoff factors, construction of strength functions of various kinds etc. However in doing so one faces two serious problems – as French and Kota [Fr-83b] state: "A problem of form, however, arises, with spectral averaging, from the initial restriction of the s.p. spectrum to a finite set of s.p. states. This leads to the level density as a superposition of configuration densities valid only for a restricted part of the spectrum. The consequence is that one loses contact with

the essentially combinatorial NIP form. Moreover, as we extend the s.p. spectrum in order to proceed to higher energies we encounter a problem of substance, namely that the variances of all the configuration distributions increase indefinitely; this, on the face of it, generates ever larger orbital admixings and spreadings, destroying the shell model stability. We shall dispose of both of these problems." The problem of form is cured by employing unitary group decompositions of the hamiltonian (and other operators) from the beginning together with the use of a moment method for constructing NIP densities. The problem of substance is cured by introducing the so called s - quantum number to catalog configurations so that distant configurations can be identified and the admixing among them are then treated separately or ignored. With this one has the subject of SAT-LSS and as stated in Chapter 1, the present thesis undertakes to study some aspects of SAT-LSS and apply the theory to problems of interest in nuclear physics and nuclear astrophysics.

3.1.1 S - decomposition

Starting with the decomposition of m-particle spaces into unitary and spherical configurations given by (2.43), a further decomposition is possible by attaching a s_α label to each spherical orbit α where s_α for lighter nuclei denotes $s\hbar\omega$ excitation value; for heavy nuclei the definition of s has to be somewhat modified. The purpose of the s quantum number is to catalog distant configurations. Fig. 3.1 gives an example. Given s^π values for the spherical orbits α, one can define the unitary orbits $\boldsymbol{\alpha}$ such that all the spherical orbits with the same s^π values belong to $\boldsymbol{\alpha}$ (in Fig. 3.1, the unitary orbits $\boldsymbol{\alpha}'$ do not satisfy this criterion). Then the corresponding unitary configurations [**m**] define uniquely the S-subspaces of the m-particle space. With this, the m-particle space can

Figure 3.1

Classification of $(ds, fp, g_{9/2})$ spherical orbits in pn case in terms of unitary orbits and the corresponding s labels. The parity and all other quantum numbers for the orbits are shown. For example $1d_{5/2}$ implies $n = 0$, $\ell = 2$, $j = 5/2$ and the major oscillator number $N = 2n + \ell = 2$ and similarly $2p_{1/2}$ correspond to $n = 1$, $\ell = 1$, $j = 1/2$, $N = 3$ etc. Given the s^π quantum numbers for the spherical orbits, the largest possible unitary orbits correspond to $\boldsymbol{\alpha}$ in the figure. The unitary orbits $\boldsymbol{\alpha}'$ are finer than $\boldsymbol{\alpha}$. For the pn case shown in the figure, the conventions defined in Sect. 3.1.4 are followed.

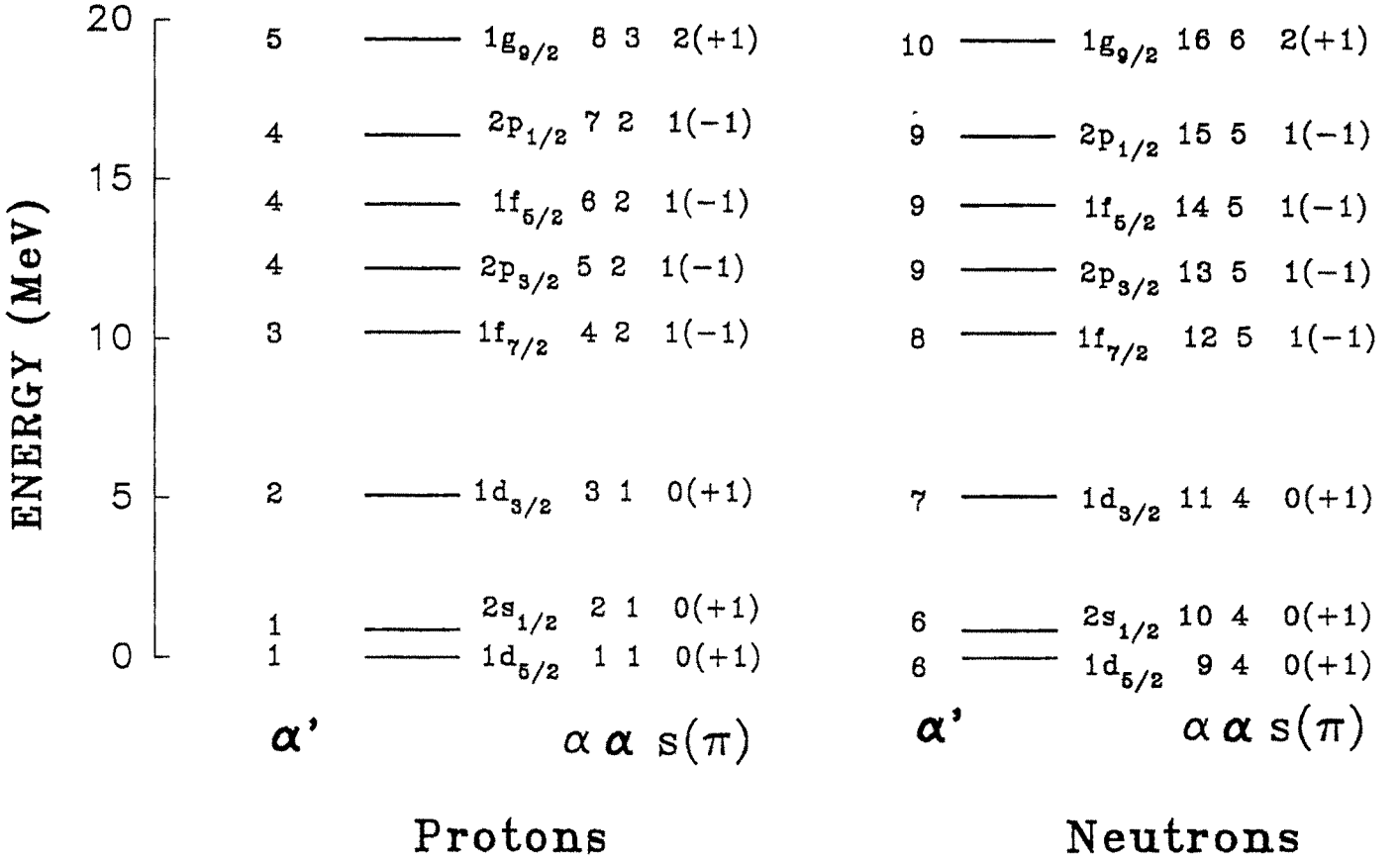
ENERGY (MeV)
20
15
10
5
0
5 — 1g9/2 8 3 2(+1)
4 — 2p1/2 7 2 1(−1)
4 — 1f5/2 6 2 1(−1)
4 — 2p3/2 5 2 1(−1)
3 — 1f7/2 4 2 1(−1)
2 — 1d3/2 3 1 0(+1)
1 — 2s1/2 2 1 0(+1)
1 — 1d5/2 1 1 0(+1)
α' α α s(π)
Protons
10 — 1g9/2 16 6 2(+1)
9 — 2p1/2 15 5 1(−1)
9 — 1f5/2 14 5 1(−1)
9 — 2p3/2 13 5 1(−1)
8 — 1f7/2 12 5 1(−1)
7 — 1d3/2 11 4 0(+1)
6 — 2s1/2 10 4 0(+1)
6 — 1d5/2 9 4 0(+1)
α' α α s(π)
Neutrons

be decomposed into S-subspaces as follows:

$$m \rightarrow \sum S^{\pi} \; ; \; S^{\pi} \rightarrow \sum [\mathrm{m}]; \; [\mathrm{m}] \rightarrow \sum \mathbf{m} \; ; \; S = \sum m_{\alpha} s_{\alpha} \qquad (3.1)$$

A similar decomposition of the hamiltonian $H = h(1) + V(2)$ is possible. The NIP hamiltonian $h = \epsilon_{\alpha} n_{\alpha}$, by definition is S - preserving. The interaction V can be decomposed into a part (V_{S-pres}) that preserves S and a part (V_{S-mix}) that mixes different S-subspaces. For example with the s.p. spectrum shown in Fig. 3.1, the $V^J_{\alpha\beta\gamma\delta}$ matrix elements that belong to V_{S-pres} are $V^J_{d_{5/2}d_{3/2}d_{5/2}s_{1/2}}$, $V^J_{d_{5/2}f_{7/2}d_{3/2}f_{5/2}}$, $V^J_{f_{5/2}p_{3/2}f_{7/2}p_{1/2}}$ etc. and those belong to V_{S-mix} are $V^J_{d_{5/2}d_{3/2}f_{7/2}f_{5/2}}$, $V^J_{d_{5/2}d_{3/2}f_{7/2}p_{3/2}}$ etc. With the S - decomposition of the m-particle space, there is a similar decomposition for the state densities (also for other densities as mentioned in Sect. 2.4); $I^m(E) = \sum_S I^{m,S}(E)$ and the moments $M_p(S)$ of $I^S(E)$ are $[\sum_{[\mathrm{m}]\in S} d([\mathrm{m}])]^{-1} \sum_{[\mathrm{m}]\in S} \langle\langle H^p \rangle\rangle^{[\mathrm{m}]}$. It is important to recognize that the fixed-S variance $\sigma^2(S) = \sigma^2(S \rightarrow S) + \sum_{S \neq S'} \sigma^2(S \rightarrow S')$ just as in (2.46, 2.47). The partial variance $\sigma^2(S \rightarrow S')$, which is due to V_{S-mix}, represents admixing between distant configurations (at least $2\hbar\omega$ away from each other) and this leads to multimodal forms for densities unlike the unimodal forms given by the CLT results in Sect. 2.3. A schematic model to understand the origin of the multimodal forms was introduced in [Fr-83b, Fr-84] and tests of some of the results of this model are given in Appendix A. Therefore in large shell model spaces either one should derive a method for incorporating the $\sigma^2(S \rightarrow S')$ partial variance corrections (i.e. V_{S-mix} effects) to the CLT results given in Sect. 2.3 or to the extent they are not harmful, just ignore them. The later is what is done in the remainder of the thesis and we will return to the former in Chapter 7. Thus by ignoring the V_{S-mix} part of the interaction $H \rightarrow h(1) + V_{S-pres} = h + V$ and in the thesis, from now onwards V stands for V_{S-pres} unless otherwise specified. Thus H is S preserving

and $I(E)$ decomposes into non-interacting partial $I^{m,S}(E)$ densities,

$$I^{H,m} = \sum_S I^{H,S}(E) = \sum_S \sum_{[\mathbf{m}]\in S} I^{H,[\mathbf{m}]}(E)$$

$$I^{H,S} \Leftrightarrow M_p(S) = \left[\sum_{[\mathbf{m}]\in S} d([\mathbf{m}])\right]^{-1} \sum_{[\mathbf{m}]\in S} d([\mathbf{m}]) M_p([\mathbf{m}]) \qquad (3.2)$$

Before going further, three points are worth mentioning and they are: (i) unlike the case with unitary configurations [m] which are defined by a group as described in Sect. 2.5, the s quantum number is not defined by a group and hence direct trace propagation for calculating $M_p(S)$ is not possible. However, as described in Sect. 2.6 $M_p([\mathbf{m}])$ given in (3.2) can be calculated using trace propagation equations; (ii) the V_{S-pres} in general admixes different unitary configurations [m] belonging to a given S and this admixing must be included while constructing the $I^{H,[\mathbf{m}]}$ densities appearing in (3.2); (iii) Eq. (3.2) extends directly to the case of expectation value densities. With the S - decomposition of the densities, we are in a position to describe the convolution results for state, spin-cutoff and occupancy densities in large shell model spaces. In the following section the state density results are described in some detail and only the final results for the last two densities are given.

3.1.2 Convolution form for state densities

In the absence of interactions, $H = h$ will produce spikes corresponding to each spherical configuration $\mathbf{m}$ at energies $\sum \epsilon_\alpha m_\alpha$ with degeneracy $\prod_\alpha \binom{N_\alpha}{m_\alpha}$. Now, under spherical configuration group decomposition, $V(= V_{S-pres})$ splits into two parts, $V = V^{[0]} + \mathbf{V}$ as given in Sect. 2.5.2; $h \rightarrow h^{[0]}$ under spherical configurations. When the interction V is turned on, the spikes will shift (due to $V^{[0]}$) and spread and admix (due to $\mathbf{V}$). Leaving aside $\mathbf{V}$, the $V^{[0]}$ part only

moves the NIP spikes without spreading or admixing. The nature of the motion due to $V^{[0]}$ is understood by decomposing $V^{[0]}$ with respect to the unitary configuration group that defines the S quantum number. Then $V^{[0]}$ decomposes into three parts as given by (2.58): (i) a scalar $V^{[0][0]}$; (ii) an effective one-body part $V^{[0][1]}$ and (iii) an irreducible two-body part $V^{[0][2]}$. Similarly $h^{[0]}$ decomposes into $h^{[0][0]}$ and $h^{[0][1]}$. The $V^{[0][0]} + V^{[0][1]}$ part of $V^{[0]}$ just renormalizes the s.p. spectrum produced by $h = h^{[0]}$ and the renormalization is a simple function, as given explicitly by (2.58), of the unitary configuration one is dealing with. However the $V^{[0][2]}$ part will produce motion of NIP spikes that are not NIP type. Thus, to the extent that one can ignore the $V^{[0][2]}$ part of $V^{[0]}$ one has $H = \mathbf{h} + \mathbf{V}$ with $\mathbf{h}$ $(= h^{[0][0]} + h^{[0][1]} + V^{[0][0]} + V^{[0][1]})$ and $\mathbf{V}$ being orthogonal to each other ((3.13) ahead gives an example). Now the normalized density $\rho(E)$ for fixed-S can be written as

$$\rho^m(E) = \langle\delta(H-E)\rangle^m \Rightarrow \langle\delta(\mathbf{h}+\mathbf{V}-E)\rangle^{\mathbf{m}}$$

$$= [d(m)]^{-1}\sum_{\mathbf{m}} d(\mathbf{m})\langle\delta(\mathbf{h}+\mathbf{V}-E)\rangle^{\mathbf{m}}$$

$$\xrightarrow[\substack{\text{each } \mathbf{m}\\ \text{subspace}}]{\substack{\text{CLT for}}} [d(m)]^{-1}\sum d(\mathbf{m})\langle\epsilon(\mathbf{m})+\mathbf{V}-E\rangle^{\mathbf{m}}$$

$$= [d(m)]^{-1}\sum d(\mathbf{m})\int\langle\mathbf{h}-x\rangle^{\mathbf{m}}\langle\mathbf{V}+x-E\rangle^{\mathbf{m}}dx$$

$$= [d(m)]^{-1}\sum I^{\mathbf{h},\mathbf{m}}\otimes\rho_{\mathcal{G}}^{\mathbf{v},\mathbf{m}}[E]$$

$$\begin{array}{l} \text{spreading variances} \\ \longrightarrow \\ \text{produced by } \mathbf{V} \text{ are} \\ \text{independent of } \mathbf{m} \end{array} \quad d^{-1}(m)\{\sum_{\mathbf{m}} I^{\mathbf{h},\mathbf{m}}\} \otimes \rho_{\mathcal{G}}^{\mathbf{v},m}[E]$$

$$= \rho^{\mathbf{h}} \otimes \rho_{\mathcal{G}}^{\mathbf{V}}[E] \tag{3.3}$$

$$\begin{aligned} \Longrightarrow I^H(E) &= \sum_S I^{\mathbf{h},S} \otimes \rho_{\mathcal{G}}^{\mathbf{V},S}[E] \\ &= \sum_S \left\{ \sum_{[\mathbf{m}]\in S} I^{\mathbf{h},[\mathbf{m}]} \otimes \rho_{\mathcal{G}}^{\mathbf{V},[\mathbf{m}]}[E] \right\}; \\ \rho_{\mathcal{G}}^{\mathbf{V},[\mathbf{m}]} \Leftrightarrow \sigma_{\mathbf{V}}([\mathbf{m}]) &= \left\{ \langle \mathbf{V}^2 \rangle^{[\mathbf{m}]} \right\}^{1/2} \\ \rho_{\mathcal{G}}^{\mathbf{V},S} \Leftrightarrow \sigma_{\mathbf{V}}(S) &= \left[\left\{ \sum_{[\mathbf{m}]\in S} d([\mathbf{m}]) \right\}^{-1} \sum_{[\mathbf{m}]\in S} d([\mathbf{m}]) \langle \mathbf{V}^2 \rangle^{[\mathbf{m}]} \right]^{1/2} \end{aligned} \tag{3.4}$$

The first two equations in (3.3) just define $\rho^m(E)$ taking into account that $V^{[0][2]}$ part is negligible. The third equality follows easily from (2.44). The fourth equality in (3.3) follows from the fact that $\mathbf{h}$ and $\mathbf{V}$ are orthogonal to each other and in the CLT limit the $\rho^{\mathbf{h}+\mathbf{V},\mathbf{m}}(E)$ will be a Gaussian with all the moments defined in terms of the centroid $\langle \mathbf{h}+\mathbf{V} \rangle^{\mathbf{m}} = \langle \mathbf{h} \rangle^{\mathbf{m}} = \epsilon(\mathbf{m})$ and variance $\langle (\mathbf{h}+\mathbf{V})^2 \rangle^{\mathbf{m}} = \langle \mathbf{h}^2 \rangle^{\mathbf{m}} + \langle \mathbf{V}^2 \rangle^{\mathbf{m}}$ which are additive with no cross term between $\mathbf{h}$ and $\mathbf{V}$; thus the CLT result given in (2.28) is applied locally. Then the local convolution form given by the fifth and sixth equalities is immediate. The seventh equality follows from the assumption of constancy of fixed-$\mathbf{m}$ variances. This leads to the result that I^H is a convolution of the NIP density $I^{\mathbf{h}}$ with the spreading Gaussian produced by $\mathbf{V}$ (in each S-subspace). Now carrying (3.3) over each S-subspace, one has the final convolution result given by (3.4); note that the S-subspaces are non-interacting. An additional fact, not mentioned before but is used in (3.3) is the feature of constancy of fixed-$\mathbf{m}$

widths. This is a well known result in SAT ([Pa-78, Wo-86] give examples) and in [Fr-83b, Fr-89a, Fr-94] it is explicitly verified that the spreading widths for $\mathbf{m}$'s that belong to fixed-S subspaces fluctuate very little from each other (the fluctuation is $\lesssim 3\%$) and its origin lies in an ensemble representation of $\mathbf{V}$ [Fr-89a, Fr-94]. Table 3.1 gives the average fixed-S spreading widths $\sigma_{\mathbf{V}}$ ((3.4) gives the definition of $\sigma_{\mathbf{V}}(S)$) in various parts of the periodic table. The results show that the widths are $\sim 6-8\ MeV$ for lighter nuclei ($A \lesssim 60$) and $\sim 2\ MeV$ for rare earth and actinide nuclei; the numbers are obtained using (2.71).

The convolution result given by (3.3) and (3.4) tacitly assumes that the internal structure of $\mathbf{V}$ does not play any role in generating smoothed state densities. All it does is to produce a *scale* which is the average spreading variance. If this is so, then all realistic interactions (in a given shell) should be highly correlated. This led us to calculate $\zeta_{\mathbf{V_1}-\mathbf{V_2}}$ for various ds-shell interactions. The results are given in the Table 3.2. As can be seen from Table 3.2, except for BARE-G and MSDI interactions, which are exceptional (BARE-G has no renormalization and MSDI is phenomenological), rest of the intearctions are highly correlated. The mass dependent UNIV-SD and BONN-J interactions are somewhat different from the rest of the interactions (PW, CW, KB, KLS-R, VY, K+12FP). Thus the results in the table indirectly justify the assumption that $\mathbf{V}$ produces a constant spreading width. This conclusion which is based on correlation coefficients, is consistent with the recent claim of Zucker and collaborators [Ab-91] who argued that as long as $V^{[0]}$ is taken care of properly, the saturation properties of nuclei can be described by any realistic interaction.

Table 3.1 Spreading widths $\sigma_{\mathbf{V}}$ (in MeV) for state densities in various parts of the periodic table. Given also in the table are also the centroid shifts $\epsilon_{\mathbf{V};J_z^2}$ (in MeV) and spreading widths $\sigma_{\mathbf{V};J_z^2}$ (in MeV) for spin-cutoff densities.

Space	Interaction	$(m_p, m_n, S)^\dagger$	$\sigma_{\mathbf{V}}$	$\epsilon_{\mathbf{V};J_z^2}$	$\sigma_{\mathbf{V};J_z^2}$
(ds)	KUO-67[i]	(2,4,0)	6.687	−0.644	6.146
		(4,4,0)	8.442	−0.837	7.800
		(6,6,0)	9.570	−0.942	8.840
	UNIV-SD[ii]	(2,4,0)	6.701	−0.681	6.171
		(4,4,0)	8.242	−0.861	7.627
		(6,6,0)	8.923	−0.921	8.254
(fp)	MWH2[iii]	(3,7,0)	5.905	−0.213	5.582
		(6,10,0)	7.846	−0.315	7.435
		(10,10,0)	8.565	−0.344	8.136
	FPM13[iv]	(3,7,0)	5.725	−0.282	5.419
		(6,10,0)	7.309	−0.391	6.928
		(10,10,0)	7.788	−0.417	7.399
(ds, fp)	KUO-7[v]	(4,4,0)	7.567	−1.077	6.993
		(4,4,1)	8.624	−1.107	8.212
		(4,4,2)	9.318	−0.995	8.993
		(6,6,0)	8.560	−1.222	7.933
		(6,6,1)	10.107	−1.219	9.583
		(6,6,2)	11.325	−1.253	10.866
		(8,8,0)	7.567	−1.007	6.993
		(8,8,1)	9.606	−1.134	9.006
		(8,8,2)	11.318	−1.237	10.809
#1	SDI[vi]	(10,10,0)	2.005	0.043	1.946
		(16,17,0)	2.071	0.030	2.013
	P + Q.Q[vi]	(10,10,0)	2.079	0.068	2.016
		(16,17,0)	2.022	0.072	1.965
#2	SDI[vi]	(10,16,0)	1.835	0.038	1.790
		(11,19,0)	1.905	0.040	1.861
	P + Q.Q[vi]	(10,16,0)	1.594	0.054	1.553
		(11,19,0)	1.640	0.058	1.598

[i][Ku-67]; [ii][Wi-84]; [iii][Mc-70]; [iv][Ri-91]; [v][Ku-71]; [vi]Appendix B
#1 $(2d_{5/2}1h_{11/2}2d_{3/2}3s_{1/2})^{m_p} \oplus (1h_{9/2}1i_{13/2}3p_{3/2}2f_{5/2}3p_{1/2})^{m_n}$;
#2 $(1h_{9/2}1i_{13/2}2f_{7/2})^{m_p} \oplus (2g_{9/2}1j_{15/2}1i_{11/2}3d_{5/2})^{m_n}$; † see Table 3 3.

Table 3.2 Correlation coefficients between V part of different *ds*-shell interactions

interaction #1	interaction #2	$\zeta_{V_1-V_2}$	interaction #1	interaction #2	$\zeta_{V_1-V_2}$
BARE-G[i]	KB[ii]	0.88	CW	KLS-R	0.98
	PW[iii]	0.87		VY	0.97
	CW[iv]	0.89		UNIV-SD	0.94
	KLS-R[v]	0.86		BONN-J	0.94
	VY[vi]	0.84		MSDI	0.81
	UNIV-SD[vii]	0.87		K+12FP	0.98
	BONN-J[viii]	0.85	KLS-R	VY	0.98
	MSDI[ix]	0.73		UNIV-SD	0.98
	K + 12FP[x]	0.87		BONN-J	0.98
KB	PW	0.99		MSDI	0.80
	CW	0.98		K +12FP	0.97
	KLS-R	0.99	VY	UNIV-SD	0.93
	VY	0.97		BONN-J	0.93
	UNIV-SD	0.92		MSDI	0.80
	BONN-J	0.92		K + 12FP	0.96
	MSDI	0.81	UNIV-SD	BONN-J	0.96
	K+12FP	0.98		MSDI	0.81
PW	CW	0.99		K+12FP	0.92
	KLS-R	0.98	BONN-J	MSDI	0.92
	VY	0.97		K+12FP	0.92
	UNIV-SD	0.92	MSDI	K+12FP	0.81
	BONN-J	0.92			
	MSDI	0.81			
	K+12FP	0.98			

All the calculations are carried out in five (m_p, m_n) spaces. The V parts of various interactions are obtained using (2.56, 2.57). The correlation coefficient $\zeta_{V_1-V_2}$ is defined by $\zeta_{V_1-V_2} = \langle V_1 V_2 \rangle^{m_p,m_n} / \{\langle V_1{}^2 \rangle^{m_p,m_n} \langle V_2{}^2 \rangle^{m_p,m_n}\}^{1/2}$ and all the traces are calculated using (2.71). The values of (m_p, m_n) are not shown in the table as ζ is found to be essentially independent of (m_p, m_n).

[i][*ds*-shell part of bare G-matrix elements of Hamada - Johnston potential obtained with $\hbar\omega = 12.5\ MeV$ [Ku-65]] ; [ii][the $3p-1h$ renormalized interaction from Hamada - Johnston potential with $\hbar\omega = 12.5\ MeV$ [Ku-65]] ; [iii][Pr-72] ; [iv][Va-77] ; [v][Ka-69] ; [vi][Va-77] ; [vii][Wi-84] ; [viii][Ji-92] ; [ix][Br-77] ; [x][Ha-71].

3.1.3 Convolution forms for spin-cutoff and occupancy densities

The convolution form (given by 3.3, 3.4) for state densities extended to spin-cutoff and occupancy densities $I^H_{J^2_Z}(E)$ and $I^H_{n_\alpha}(E)$ respectively [Fr-89b, Fr-94],

$$I^H_K(E) = \langle\langle K\delta(H-E)\rangle\rangle^m$$

$$= \sum_S I^{\mathrm{h},S}_K \otimes \rho^{\mathbf{V},S}_{K:\mathcal{G}}[E]\,;\ \ K = J^2_Z \ \ or \ \ n_\alpha$$

$$\rho^{\mathbf{V},S}_{K}(x) = \frac{\langle K\delta(V-x)\rangle^{m,S}}{\langle K\rangle^{m,S}}\ ;$$

$$\rho^{\mathbf{V},S}_{K:\mathcal{G}}(E) \ \Leftrightarrow \ \left\{\begin{array}{lcl} \epsilon_{\mathbf{V}:K}(S) & = & \left\{\sum\limits_{[\mathrm{m}]\in S} d([\mathrm{m}])\langle K\mathbf{V}\rangle^{[\mathrm{m}]}\right\} \Big/ \left\{\sum\limits_{[\mathrm{m}]\in S} d([\mathrm{m}])\langle K\rangle^{[\mathrm{m}]}\right\} \\ \sigma_{\mathbf{V}:K}(S) & = & \left[\left\{\sum\limits_{[\mathrm{m}]\in S} d([\mathrm{m}])\langle K\mathbf{V}^2\rangle^{[\mathrm{m}]}\right\} \Big/ \left\{\sum\limits_{[\mathrm{m}]\in S} d([\mathrm{m}])\langle K\rangle^{[\mathrm{m}]}\right\} \right. \\ & & \left. - \{\epsilon_{\mathbf{V}:K}(S)\}^2\right]^{1/2} \end{array}\right. \tag{3.5}$$

The K - centroids $\epsilon_{\mathbf{V}:K}(S)$ (in fact centroid shifts with respect to the $\rho^{\mathbf{V}}_{\mathcal{G}}$ centroid $\epsilon_{\mathbf{V}} = \langle\mathbf{V}\rangle = 0$) and widths $\sigma_{\mathbf{V}:K}(S)$ define the $\rho^{\mathbf{V},S}_{K:\mathcal{G}}(E)$ spreading Gaussian densities. One can rewrite (3.5) in a slightly different form by using the unitary configurations [m] from the beginning,

$$\begin{aligned} I^H_K(E) &= \sum_S \left\{\sum_{[\mathrm{m}]\in S} I^{H,[\mathrm{m}]}_K(E)\right\} \\ &= \sum_S \left\{\sum_{[\mathrm{m}]\in S} I^{\mathrm{h},[\mathrm{m}]}_K \otimes \rho^{\mathbf{V},[\mathrm{m}]}_{K:\mathcal{G}}[E]\right\}; \\ \rho^{\mathbf{V},[\mathrm{m}]}_K(y) &= \langle K\delta(\mathbf{V}-y)\rangle^{[\mathrm{m}]}/\langle K\rangle^{[\mathrm{m}]}; \end{aligned}$$

$$\rho^{\mathbf{V},[\mathrm{m}]}_{K:\mathcal{G}} \Leftrightarrow \begin{cases} \epsilon_{\mathbf{V}:K}([\mathrm{m}]) &= \langle K\mathbf{V}\rangle^{[\mathrm{m}]}/\langle K\rangle^{[\mathrm{m}]} \\ \sigma_{\mathbf{V}:K}([\mathrm{m}]) &= \left[\langle K\mathbf{V}^2\rangle^{[\mathrm{m}]}/\langle K\rangle^{[\mathrm{m}]} - \{\epsilon_{\mathbf{V}:K}([\mathrm{m}])\}^2\right]^{1/2} \end{cases} \tag{3.6}$$

The form given in (3.6) for I^H_K is employed in Chapter 4 for reasons that are explained there. Modifications of the results given in (3.5, 3.6) in the cases $\langle K\rangle^{\mathrm{m}} = 0$ is straightforward. For the occupancy densities $K = n_\alpha$ it is easily seen that the centroid shifts $\epsilon_{\mathbf{V}:n_\alpha}$ are zero and in addition the widths $\sigma_{\mathbf{V}:n_\alpha}$ are very close to $\sigma_{\mathbf{V}}$; (2.72) enables one to calculate $\sigma_{\mathbf{V}:n_\alpha}([\mathrm{m}])$ and $\sigma_{\mathbf{V}:n_\alpha}(S)$. For the spin-cutoff densities $I^H_{J^2_Z}(E)$, the centroid shifts $\epsilon_{\mathbf{V}:J^2_Z}$ are not zero and they can be calculated using (2.71). Similarly the spin-cutoff spreading variances can be calculated using (2.71 - 2.73). Table 3.1 gives the average fixed-S spin-cutoff centroid shifts $\epsilon_{\mathbf{V}:J^2_Z}$ and spreading widths $\sigma_{\mathbf{V}:J^2_Z}$. One striking result that follows from Table 3.1 is that the spin-cutoff variances are consistently smaller than the state density variances and the difference is $\sim 10\%$. This result is used in Chapter 4.

3.1.4 Moment methods and convolution forms for NIP state, spin-cutoff and occupancy densities

In order to apply (3.3) - (3.6), it is essential to have good methods for constructing NIP densities $I^h(E)$ and their S - decompositions; methods for calculating the centroids and variances of the spreading functions are already given. In principle one can construct NIP densities exactly by using spherical orbits and spherical configurations, i.e. by employing the well known direct counting method [Hi-69]. However this method suffers from several problems: (i) the method becomes very slow with increasing number of spherical orbits,

typically, say the number of orbits ≥ 6; (ii) the method will not yield information about the underlying structures that generate the NIP densities; (iii) it will not give any explanation to the connection between the CLT Gaussian form and Bethe's exponential $exp\sqrt{aE}$ form for the densities. Moment methods (based on calculating the moments of the distributions and then using Edgeworth expansion (2.8)) cure these problems and enables one to construct the NIP densities rapidly and produce smoothed forms for the densities. The moment methods are easy to apply since NIP densities defined over a particular unitary configuration can be written as a multiple convolution of the densities defined over each unitary orbit. From now onwards, in this section, without loss of generality, $h = \mathrm{h}$.

With the decomposition (3.1) of the spectroscopic space, the NIP state density $I^h(E)$ and its decompositions are (assuming that there are L unitary orbits) [Fr-89a, Fr-94],

$$I^{h,m}(E) = \langle\langle \delta(h-E)\rangle\rangle^m = d(m)\langle \delta(h-E)\rangle^m = \sum_{[\mathrm{m}]} \langle\langle \delta(h-E)\rangle\rangle^{[\mathrm{m}]}$$

$$= \left[\sum_{[\mathrm{m}]} I^{h,[\mathrm{m}]}(E)\right] = \sum_S \left\{ \sum_{[\mathrm{m}]\in S} I^{h,[\mathrm{m}]}(E)\right\} = \sum_S I^{h,S}(E) \qquad (3.7)$$

$$I^{h,[\mathrm{m}]}(E) = I^{h\boldsymbol{\alpha}}_{N_{\boldsymbol{\alpha}}} \otimes I^{h\boldsymbol{\beta}}_{N_{\boldsymbol{\beta}}} \otimes ..... \otimes I^{h\mathbf{L}}_{N_{\mathbf{L}}}\ [E] \qquad (3.8)$$

In deriving (3.8), the following decomposition of the NIP hamiltonian is used: $h = \sum \epsilon_\alpha n_\alpha = \sum_\alpha h_\alpha = \sum_{\boldsymbol{\alpha}} h_{\boldsymbol{\alpha}} = \sum_{\boldsymbol{\alpha}} \left\{ \sum_{\alpha\in\boldsymbol{\alpha}} h_\alpha \right\}$. The first four central moments $\mathcal{M}_r$ of single unitary orbit densities $I^{h\boldsymbol{\alpha}}_{N_{\boldsymbol{\alpha}}}$ can be obtained using (2.63, 2.64, 2.67). The convolution form in (3.8) implies that the cumulants of $I^{h,[\mathrm{m}]}$ are sum of the cumulants of $I^{h\boldsymbol{\alpha}}_{N_{\boldsymbol{\alpha}}}$. Applying the CLT, the Edgeworth corrected

Gaussian representation for $I^{h,[\mathrm{m}]}(E)$ can be constructed and hence $I^{h,S}(E)$ and $I^{h,m}(E)$. Eqs. (3.7, 3.8) extend to the more complicated expectation value densities $I^h_K(E)$. For example the occupancy density and its decompositons are [Fr-89b, Fr-94]

$$I^{h,m}_{n_\alpha}(E) = \langle\langle n_\alpha \delta(h-E)\rangle\rangle^m = \sum_{[\mathrm{m}]} \langle\langle n_\alpha \delta(h-E)\rangle\rangle^{[\mathrm{m}]} = \sum_{[\mathrm{m}]} I^{h,[\mathrm{m}]}_{n_\alpha}(E)$$

$$= \sum_S \left\{ \sum_{[\mathrm{m}]\in S} I^{h,[\mathrm{m}]}_{n_\alpha}(E) \right\} = \sum_S I^{h,S}_{n_\alpha}(E); \tag{3.9}$$

$$I^{h,[\mathrm{m}]}_{n_\alpha}(E) = I^{h\boldsymbol{\alpha}}_{N_{\boldsymbol{\alpha}};n_\alpha} \otimes I^{h\boldsymbol{\beta}}_{N_{\boldsymbol{\beta}}} \otimes \ldots\ldots \otimes I^{h\mathrm{t}}_{N_\mathrm{t}} \otimes \ldots\ldots \otimes I^{h\mathrm{L}}_{N_\mathrm{L}} \ [E] \ \text{ for } \alpha \in \boldsymbol{\alpha}. \tag{3.10}$$

In applying the convolution result (3.10) for orbit $\tau \in \mathrm{t}$, the suffix n_τ in the R.H.S. of (3.10) should be attached to $I^{h\mathrm{t}}_{N_\mathrm{t}}$, i.e. $I^{h\mathrm{t}}_{N_\mathrm{t}} \to I^{h\mathrm{t}}_{N_\mathrm{t};n_\tau}$ and $I^{h\boldsymbol{\alpha}}_{N_{\boldsymbol{\alpha}},n_\alpha} \to I^{h\boldsymbol{\alpha}}_{N_{\boldsymbol{\alpha}}}$. The moments of $I^{h\boldsymbol{\alpha}}_{N_{\boldsymbol{\alpha}};n_\alpha}(E)$ follow by the parametric differentiation of the moments of $I^{h\boldsymbol{\alpha}}_{N_{\boldsymbol{\alpha}}}(E)$ as given by (2.34). Thus once again applying CLT, Edgeworth corrected Gaussian representation for $I^{h,[\mathrm{m}]}_{n_\alpha}(E)$ can be constructed and hence $I^{h,S}_{n_\alpha}(E)$ and $I^{h,m}_{n_\alpha}(E)$. Extension of (3.9) to J^2_Z operator is immediate,

$$I^{h,m}_{J^2_Z}(E) = \langle\langle J^2_Z \delta(h-E)\rangle\rangle^m = \sum_S I^{h,S}_{J^2_Z}(E) = \sum_S \left[\sum_{[\mathrm{m}]\in S} I^{h,[\mathrm{m}]}_{J^2_Z}(E) \right] \tag{3.11}$$

The moments of $I^{h,[\mathrm{m}]}_{J^2_Z}(E)$ follow from the convolution result given in (3.8) with $h \to h + \lambda J_Z$ and carrying out double parametric differention of resulting moments as given by (2.35). Alternatively noting that $J_Z = \sum_\alpha J_Z(\alpha)$ and $\langle J^2_Z\rangle = \sum_\alpha \langle J^2_Z(\alpha)\rangle$, one can apply the convolution result (3.10) for $J^2_Z(\alpha)$ (in place of n_α) and this then will yield the moments of $I^{h,[\mathrm{m}]}_{J^2_Z}(E)$.

3.1.5 Summary of convolution results and conventions for pn systems

To summarize, in SAT-LSS as given by (3.3) - (3.6) the state, spin-cutoff and occupancy densities are sum of partial non-interacting fixed-S densities with density for each S taking a convolution form. Given $H = \mathbf{h} + \mathbf{V}$, the fixed-$S$ densities are convolution of NIP densities produced by $\mathbf{h}$ with the spreading Gaussuian produced by $\mathbf{V}$. The spreading Gaussians are determined by first two moments viz. by centroids and variances. In addition the moment method also allows to construct NIP densities as there are further convolution forms for partial NIP densities as given by (3.7 - 3.11). Our purpose in this chapter is to test (in a comprehensive manner) two important aspects of SAT-LSS and they are: (i) establishing that $V^{[0][2]}$ is small for intearctions all across the periodic table; (ii) test of moment methods for constructing the NIP densities and their S - decompositions. The results of these studies are given in Sects. 3.2 and 3.3 respectively. In the examples given in Sects 3.2 and 3.3 as well as in Chapters 3 - 6 pn systems are dealt with or in other words the pn formalism (but not the isospin formalism) is used. All the results given in Chapter 2 and in Sect. 3.1 apply directly to the pn case with the following conventions. The conventions given below are used throughout the thesis unless otherwise specified.

For pn systems, with protons and neutrons occupying spherical orbits α with angular momentum j_α, the following conventions are used. Let us assume that there are k_p number of proton orbits and k_n number of neutron orbits. Then the orbit label α takes values $\alpha = 1, 2, ..., k_p + k_n$ with α = 1,2,...k_p being protron orbits α(p) and $\alpha = k_p + 1,\ k_p + 2$,...$k_p + k_n$ being neutron

orbits α(n) as shown for example in Fig. 3.1. A pn configuration ($\mathbf{m_p}$, $\mathbf{m_n}$) = (m_p^1, m_p^2, ..., $m_p^{k_p}$, m_n^1, m_n^2,...,$m_n^{k_n}$) then corresponds to the configuration $\mathbf{m}$ = (m_1, m_2,...$m_{k_p+k_n}$) with $m_1 = m_p^1$, $m_2 = m_p^2$, ..., $m_{k_p} = m_p^{k_p}$, $m_{k_p+1} = m_n^1$, $m_{k_p+2} = m_n^2$, ..., $m_{k_p+k_n} = m_n^{k_n}$, where $m_p^{\alpha(p)}$ and $m_n^{\alpha(n)}$ are proton and neutron numbers in orbits α(p) and $\alpha(n)$ respectively and m_α is number of particles in the orbit α. Similarly defined are the SPE ϵ_α, the orbit degeneracies N_α, $N_{\boldsymbol{\alpha}}$, $V_{\alpha\beta}$, $V_{\boldsymbol{\alpha\beta}}$ etc. In the pn case, the eigenstates of h are given by the spherical configurations $\mathbf{m} = (\mathbf{m_p}, \mathbf{m_n})$ with energies $\epsilon(\mathbf{m_p}, \mathbf{m_n}) = \epsilon(\mathbf{m}) = \sum m_\alpha \epsilon_\alpha$ and dimensionalities $d(\mathbf{m_p}, \mathbf{m_n}) = d(\mathbf{m}) = \prod_\alpha \begin{pmatrix} N_\alpha \\ m_\alpha \end{pmatrix}$. Let us consider the example of 4 protons and 6 neutrons in the space defined by the spherical orbits $1d_{5/2}$, $2s_{1/2}$, $1d_{3/2}$, $1f_{7/2}$, $2p_{3/2}$, $2p_{1/2}$, $1f_{5/2}$. With the conventions defined above, α = 1, 2, 3, 4, 5, 6, 7, 8, 9, 10, 11, 12, 13, 14 correspond to $1d_{5/2}$, $2s_{1/2}$, $1d_{3/2}$, $1f_{7/2}$, $2p_{3/2}$, $2p_{1/2}$, $1f_{5/2}$, $1d_{5/2}$, $2s_{1/2}$, $1d_{3/2}$, $1f_{7/2}$, $2p_{3/2}$, $2p_{1/2}$ and $1f_{5/2}$ orbits respectively; the first seven orbits are for protons and the next seven are for neutrons. The configuration (4,0,0,0,0,0,0,6,0,0,0,0,0,0) correspond to $(1d_{5/2})^{4p}(1d_{5/2})^{6n}$ and similarly $(3,0,1,0,0,0,0,4,0,0,2,0,0,0)$ correspond to $(1d_{5/2})^{3p}(1d_{3/2})^{1p}(1d_{5/2})^{4n}(1f_{7/2})^{2n}$ etc. Also N_α = 6, 2, 4, 8, 4, 2, 6, 6, 2, 4, 8, 4, 2, 6 for $\alpha = 1, 2, 3, ..., 14$. Finally it should be added that for the case of unitary orbits in pn case, the unitary orbits should be chosen such that the spherical orbits belong to a unitary orbit are all either proton orbits or neutron orbits; Fig. 3.1 and the footnotes to Table 3.3 ahead give examples. In the example considered above, choosing ds and fp orbits to be unitary orbits, $\boldsymbol{\alpha}$ = 1, 2, 3, 4 correspond to ds, fp, ds and fp with $N_{\boldsymbol{\alpha}}$ = 12, 20, 12, 20 respectively; the first two orbits are for protons and the next two are for neutrons. The unitary configuration [4,0,6,0] corresponds to $(ds)^{4p}(ds)^{6n}$ and similarly [3,1,4,2] corresponds to $(ds)^{3p}(fp)^{1p}(ds)^{4n}(fp)^{2n}$ etc.

3.2 Test of the smallness of $V^{[0][2]}$ part of various interactions

In this section, a large variety of nuclear hamiltonians ($H = h(1) + V(2)$) are considered in spectroscopic spaces relevant for nuclei in various parts of the periodic table (*ds*, *fp*, *ds-fp*, *ds-fp-sdg* etc.) and employing a norm that defines sizes of operators (footnote #3 in Chapter 1), it is shown that $V^{[0][2]}$, the non-NIP like part of $V^{[0]}$, is indeed small in all cases considered. Similar results are obtained in [Fr-83b, Fr-89a] by considering some limited examples and the present exercise aims at completeness; results of this section are first reported in [Ko-92b]. Given the one plus two-body hamiltonian $H = h(1) + V(2)$ defined by the SPE ϵ_α and TBME $V^J_{\alpha\beta\gamma\delta}$, using (2.56, 2.57) the decomposition $H = \left\{h(1) + V^{[0]}\right\} + \mathbf{V}$ is carried out with $V^{[0]}$ defined by $V_{\alpha\beta}$ matrix elements (2.50). As described in Sect. 3.1, $H \rightarrow \mathbf{h} + \mathbf{V}$; $h(1) + V^{[0]} \rightarrow \mathbf{h} = \left[h^{[0][0]} + V^{[0][0]}\right] + \left[h^{[0][1]} + V^{[0][1]}\right]$ provided $V^{[0][2]}$ is neglected. The decompositon of $h(1) + V^{[0]}$ into unitary tensor parts follows from (2.58) with the transcription $\mathcal{E}_\alpha \rightarrow \epsilon_\alpha$, $C_{\alpha\beta} \rightarrow V_{\alpha\beta}$, $\mathcal{E}_{\boldsymbol{\alpha}} \rightarrow \epsilon_{\boldsymbol{\alpha}}$, $C_{\boldsymbol{\alpha\beta}} \rightarrow V_{\boldsymbol{\alpha\beta}}$, $\mathcal{E}^{[1]}_\alpha \rightarrow \epsilon^{[1]}_\alpha$ and $\mathcal{A}^{[1]} \rightarrow H^{[0][1]}$.

In order to establish that the $V^{[0][2]}$ part of $\{h + V^{[0]}\}$ is small compared to the $\{h^{[0][1]} + V^{[0][1]}\}$ part ($\{h^{[0][0]} + V^{[0][0]}\}$ part of $\mathbf{h}$ behaves as a scalar (number) with respect to unitary configurations and hence this part need not be considered in the calculation of norms), the unitary norm [Fr-72, Fr-83b] which gives the measure of the size of an operator is employed. In the present case, the fixed unitary configuration norm $|\mathcal{O}|_{[\mathbf{m}]}$ of an operator $\mathcal{O}$ (which do not have [**0**] tensor part) is defined simply by $|\mathcal{O}|^2_{[\mathbf{m}]} = \langle \mathcal{O}^\dagger \mathcal{O} \rangle^{[\mathbf{m}]}$; the unitary configuration trace on the R.H.S. follows from the results given in Sect. 2.6.

The explicit propagation equations for the squares of norms of $h^{[0][1]}$, $V^{[0][1]}$, $H^{[0][1]} = h^{[0][1]} + V^{[0][1]}$ and $V^{[0][2]}$ are given by,

$$\begin{aligned}
\left|h^{[0][1]}\right|^2_{[\mathbf{m}]} &= \sum_{\boldsymbol{\alpha}} \frac{m_{\boldsymbol{\alpha}} m^{\times}_{\boldsymbol{\alpha}}}{N_{\boldsymbol{\alpha}\boldsymbol{\alpha}}} \sum_{\alpha} N_{\alpha} \left\{\epsilon^{[1]}_{\alpha}\right\}^2 \\
\left|V^{[0][1]}\right|^2_{[\mathbf{m}]} &= \sum_{\boldsymbol{\alpha}} \frac{m_{\boldsymbol{\alpha}} m^{\times}_{\boldsymbol{\alpha}}}{N_{\boldsymbol{\alpha}\boldsymbol{\alpha}}} \sum_{\alpha} N_{\alpha} \left\{\zeta^{[1]}_{\alpha}([\mathbf{m}])\right\}^2 \\
\left|H^{[0][1]}\right|^2_{[\mathbf{m}]} &= \sum_{\boldsymbol{\alpha}} \frac{m_{\boldsymbol{\alpha}} m^{\times}_{\boldsymbol{\alpha}}}{N_{\boldsymbol{\alpha}\boldsymbol{\alpha}}} \sum_{\alpha} N_{\alpha} \left\{\xi^{[1]}_{\alpha}([\mathbf{m}])\right\}^2 \\
\left|V^{[0][2]}\right|^2_{[\mathbf{m}]} &= \sum_{\boldsymbol{\alpha} \geq \boldsymbol{\beta}} \frac{m_{\boldsymbol{\alpha}\boldsymbol{\beta}} m^{\times}_{\boldsymbol{\alpha}\boldsymbol{\beta}}}{N_{\boldsymbol{\alpha}\boldsymbol{\beta}\boldsymbol{\alpha}\boldsymbol{\beta}}} [1 + \delta_{\boldsymbol{\alpha}\boldsymbol{\beta}}]^{-1} \sum_{\substack{\alpha \in \boldsymbol{\alpha} \\ \beta \in \boldsymbol{\beta}}} (V^{[0][2]}_{\alpha\beta})^2 N_{\alpha\beta}
\end{aligned} \tag{3.12}$$

It is essential to recognize that the different $[\boldsymbol{\nu}]$ tensor parts of $h + V^{[0]}$ are orthogonal to each other with respect to the fixed-$[\mathbf{m}]$ norm defined above. In general for one plus two-body operators $\mathcal{A} = \sum_{[\boldsymbol{\nu}]} \mathcal{A}^{[\boldsymbol{\nu}]}$ and $\mathcal{B} = \sum_{[\boldsymbol{\nu}]} \mathcal{B}^{[\boldsymbol{\nu}]}$,

$$\langle \mathcal{A}\mathcal{B} \rangle^{[\mathbf{m}]} = \langle \mathcal{A}^{[\mathbf{0}]} \mathcal{B}^{[\mathbf{0}]} \rangle^{[\mathbf{m}]} + \langle \mathcal{A}^{[\mathbf{1}]} \mathcal{B}^{[\mathbf{1}]} \rangle^{[\mathbf{m}]} + \langle \mathcal{A}^{[\mathbf{2}]} \mathcal{B}^{[\mathbf{2}]} \rangle^{[\mathbf{m}]}. \tag{3.13}$$

Applying (3.13), gives the important result that in $h + V^{[0]} \rightarrow H^{[0][1]} + V^{[0][2]}$, $V^{[0][2]}$ is orthogonal to $H^{[0][1]}$ and therefore the smallness of $V^{[0][2]}$ can be established by comparing the norm of $H^{[0][1]} + V^{[0][2]}$ with that of $V^{[0][2]}$. Finally, fixed-S norms are defined in terms of fixed-$[\mathbf{m}]$ norms as follows,

$$|K|^2_S = \left[\sum_{[\mathbf{m}] \in S} d([\mathbf{m}])\right]^{-1} \left[\sum_{[\mathbf{m}] \in S} d([\mathbf{m}]) |K|^2_{[\mathbf{m}]}\right] \tag{3.14}$$

where $K = h^{[0][1]}$, $V^{[0][1]}$, $H^{[0][1]}$ or $V^{[0][2]}$.

The unitary decomposition and calculation of norms are carried out for the following cases and they span the entire periodic table:

(*i*) The *ds*-shell interactions :

(a) Chung Wildenthal interaction (given in [Va-77]) (CW) with ^{17}O energies (−4.15, 0.93, −3.28) MeV for ($1d_{5/2}$, $1d_{3/2}$, $2s_{1/2}$) orbits.

(b) Preedom Wildenthal interaction [Pr-72] (PW) with ^{17}O energies (−4.15, 0.93, −3.28) MeV for ($1d_{5/2}$, $1d_{3/2}$, $2s_{1/2}$) orbits.

(c) Universal−*sd* interaction (UNIV-SD) of Wildenthal [Wi-84] where the two-body matrix elements have A-dependence $(18/A)^{0.3}$ and the SPE are (−3.948, 1.647, −3.164) MeV for ($1d_{5/2}$, $1d_{3/2}$, $2s_{1/2}$) orbits.

(d) Interaction (BONN-J) derived from Bonn-A potential by Jiang et al [Ji-92]. The SPE are (0.000, 5.080, 0.870) MeV for ($1d_{5/2}$, $1d_{3/2}$, $2s_{1/2}$) orbits.

(e) Pairing plus quadrupole - quadrupole (P + Q.Q) interaction (given in Appendix B) with ^{17}O energies (−4.15, 0.93, −3.28) MeV for ($1d_{5/2}$, $1d_{3/2}$, $2s_{1/2}$) orbits.

(*ii*) fp-shell interactions :

(a) The McGrory, Wildenthal and Halbert interaction as modified by Sharma and Bhatt (MWH2) [Mc-70] with ^{41}Ca energies (−8.364, −6.264, −1.864, −4.464) MeV for ($1f_{7/2}$, $2p_{3/2}$, $1f_{5/2}$, $2p_{1/2}$) orbits.

(b) FPM13 interaction of Richter et al [Ri-91] where TBME have the scale factor $(42/A)^{0.35}$ and SPE are (−8.364, −6.333, −2.154, −4.407) MeV for ($1f_{7/2}$, $2p_{3/2}$, $1f_{5/2}$, $2p_{1/2}$) orbits.

(*iii*) ($2p_{3/2}$, $1f_{5/2}$, $2p_{1/2}$, $1g_{9/2}$) space interaction KBB which is a modified version of the KUO interaction [Ku-69]; the SPE are (0.000, 0.780, 1.080,

3.000) MeV respectively.

(*iv*) ($1f_{7/2}$, $1f_{5/2}$, $2p_{3/2}$, $2p_{1/2}$, $1d_{5/2}$, $1d_{3/2}$, $2s_{1/2}$) space with Kuo interaction KUO-7; the $7(ds - fp)$ - orbit part of the KUO-10 orbit interaction defined in the 10-orbit ($1f_{7/2}$, $1f_{5/2}$, $2p_{3/2}$, $2p_{1/2}$, $1d_{5/2}$, $1d_{3/2}$, $2s_{1/2}$, $1p_{3/2}$, $1p_{1/2}$, $1s_{1/2}$) space [Ku-71]. The SPE (in MeV) are (9.380, 15.570, 11.400, 13.410, −4.150, 0.930, −3.280) respectively for the above seven fp and ds orbits. They derive from the p-h spectrum of ^{16}O as given in [Sp-65]; see also the discussion following KUO-12 interaction.

(*v*) ($1d_{5/2}$, $2s_{1/2}$, $1d_{3/2}$, $1f_{7/2}$, $2p_{3/2}$, $1f_{5/2}$, $2p_{1/2}$, $1g_{9/2}$, $2d_{5/2}$, $1g_{7/2}$, $3s_{1/2}$, $2d_{3/2}$) space with KUO interaction KUO-12; 12-orbit (ds, fp, sdg) part of the KUO-15 orbit interaction defined in the 15-orbit ($1s_{1/2}$, $1p_{3/2}$, $1p_{1/2}$, $1d_{5/2}$, $2s_{1/2}$, $1d_{3/2}$, $1f_{7/2}$, $2p_{3/2}$, $1f_{5/2}$, $2p_{1/2}$, $1g_{9/2}$, $2d_{5/2}$, $1g_{7/2}$, $3s_{1/2}$, $2d_{3/2}$) space [Ku-71]. The SPE (in MeV) are (−4.150, −3.820, 0.930, 7.210, 9.230, 13.400, 11.240, 17.780, 22.460, 21.780, 23.780, 24.380). The energies of the first 7-orbits derive from the energies of the p-h spectrum of ^{16}O as given in [Sp-65]. The $g_{9/2}$ orbit is put 1 MeV above $f_{5/2}$ orbit, ($g_{7/2} - g_{9/2}$) separation is chosen to be 4 MeV and the energies of $2d_{5/2}$, $3s_{1/2}$ and $2d_{3/2}$ orbits are chosen to be that of ^{116}Sn as given in [Bo-85]. In addition the $ds - fp$ separation is increased by Δ_1 MeV and $fp - sdg$ separation by Δ_2 MeV where the origin and the values of (Δ_1, Δ_2) are given in the footnote below [1].

[1] While dealing with ds-shell nuclei with KUO-10 orbit interaction and ds and fp-shell nuclei with KUO-15 orbit interaction, for many purposes one can eliminate the closed (for $S = 0$ configurations) s and p shells. However this introduces renormalization of the resulting 7 and 12 orbit interaction hamiltonians. The one of consequence in the present exercise is the renormalization of h. Let us consider the 10 to 7 orbit reduction with s, p, ds and fp defining the unitary orbits $\alpha = 1, 2, 3$ and 4 respectively (for both protons and neutrons). By eliminating s and p orbits, one should take into account the $ds - fp$ splitting produced

(*vi*) Rare-earth nuclei with Surface Delta Interaction (SDI) and P + Q.Q interaction; definitions of these interactions are given in Appendix B. The SPE are from zero deformation Nilsson energies [Bo-75]. For example, the SPE for the rare-earth nucleus $^{168}_{68}Er_{100}$ are (41.523, 42.194, 43.100, 44.554, 44.841) MeV and (48.475, 49.137, 49.910, 51.410, 51.778, 52.826) MeV for ($1g_{7/2}$, $2d_{5/2}$, $1h_{11/2}$, $2d_{3/2}$, $3s_{1/2}$) proton orbits and ($2f_{7/2}$, $1h_{9/2}$, $1i_{13/2}$, $3p_{3/2}$, $2f_{5/2}$, $3p_{1/2}$) neutron orbits respectively. Formulas for the strengths of SDI and P + Q.Q interactions are given in Appendix B.

(*vii*) Actinide nuclei with SDI and P + Q.Q interactions. The SPE are from zero deformation Nilsson energies [Bo-75]. For example, the SPE for the actinide nucleus $^{239}_{92}U_{147}$ are (42.745, 43.555, 43.786, 46.445, 47.023, 48.163) MeV and (48.825, 50.362, 50.445, 51.569, 52.601, 53.225, 53.667) MeV for ($1h_{9/2}$, $1i_{13/2}$, $2f_{7/2}$, $2f_{5/2}$, $2p_{3/2}$, $2p_{1/2}$) proton orbits and ($2g_{9/2}$,

---

by interactions of valence (ds, fp) particles with s^4p^{12} core and also the single particle splittings produced by this interaction Both these quantities follow easily [Fr-94] from $V_{\alpha\beta}$ and $V_{\alpha\beta}$ by using (2.58). The $ds - fp$ separation Δ is given by $\Delta = 2(V_{1p4_p} - V_{1p3_p}) + 6(V_{2p4_p} - V_{2p3_p}) + 2(V_{1n4_n} - V_{1n3_p}) + 6(V_{2n4_p} - V_{2n3_p})$. Similarly the s.p. energies $\epsilon^{[1]}_\beta$ produced by the interaction of valence particles with s^4p^{12} core are given by $h^{[1]} = \sum_\beta \epsilon^{[1]}_\beta n_\beta$; $\epsilon^{[1]}_\beta = 2\epsilon^{[1],s}_\beta(pp) + 6\epsilon^{[1],p}_\beta(pp) + 2\epsilon^{[1],s}_\beta(pn) + 6\epsilon^{[1],p}_\beta(pn)$. With KUO -10 orbit interaction $\Delta = 7.83\ MeV$ and $\epsilon^{[1]}_\beta = -1.73,\ 3.31,\ -1.43,\ -0.55,\ 4.30,\ -4.01,\ -2.68\ MeV$ for the orbits $d_{5/2}$, $d_{3/2}$, $s_{1/2}$, $f_{7/2}$, $f_{5/2}$, $p_{3/2}$, $p_{1/2}$ respectively. Similarly by extending the above results for the 15-orbit case give $ds - fp$ separation $\Delta_1 = 5.66\ MeV$ and fp-sdg separation $\Delta_2 = 3.38\ MeV$. The $\epsilon^{[1]}_\beta$ for ($d_{5/2}$, $s_{1/2}$, $d_{1/2}$) orbits are (-0.75, -1.35, 1.80) MeV, for ($f_{7/2}$, $p_{3/2}$, $f_{5/2}$, $p_{1/2}$) orbits are (0.24, -3.25, 2.70, -2.59) MeV and for ($g_{9/2}$, $d_{5/2}$, $g_{7/2}$, $s_{1/2}$, $d_{3/2}$) orbits are (1.12, -3.45, 3.12, -3.77, -1.98) MeV. The SPE produced by the interaction should be added to the primary energy which, in oscillator shell n, should be $(n + 3/2)\hbar\omega/2$. However the resulting SPE which become ϵ_α for 7 and 12-orbit interactions are not close to the ^{17}O energies given in [Sp-65]. Therefore in the present calculations these energies are replaced by ^{17}O energies and the Δ's produced by the interaction. These then give the $\epsilon^{[1]}_\alpha$ in Table 3.5 for KUO-7 and KUO-12 interactions. It is useful to note that the Δ's play no role in the norms calculations presented in Table 3.6.

$1j_{15/2}$, $1i_{11/2}$, $3d_{5/2}$, $2g_{7/2}$, $4s_{1/2}$, $3d_{3/2}$) neutron orbits respectively. Formulas for the strengths of SDI and P + Q.Q interactions are given in Appendix B.

Results of the unitary decompositions (carried out in pn spaces) are cataloged in Tables 3.3 - 3.5 and Figs. 3.2a - 3.2c. In Tables 3.3, 3.4 the SPE ϵ_{α} and TBME $V_{\alpha\beta}$ respectively that shifts the location of unitary configurations [m] (the unitary orbits are defined in the footnote of Table 3.3) are given. Although they play no role in the present investigation (i.e. establishing that $V^{[0][2]}$ part is negligible), it is useful to point out that they contribute to the backshifting of the state density. Table 3.5 gives the primary traceless SPE $\epsilon_{\alpha}^{[1]}$ and the renormalized (due to $V(2)$) energies $\xi_{\alpha}^{[1]}$; the later depend on [m] and examples for some selected [m] are shown in the table. It is striking to note that in almost all cases (exceptions being P + Q.Q interaction and in other cases those with $j = 1/2$ orbit) the renormalized energies are obtained essentially by shifting the primary energies, i.e. the $\epsilon_{\alpha}^{[1]}$ and the induced energies given by $\xi_{\alpha}^{[1]}([\mathrm{m}])$ are highly correlated. In Figs. 3.2a - 3.2c, the $V_{\alpha\beta}$ matrix elements of $V^{[0]}$ and $V^{[0][2]}$ are compared for the pp and pn parts of various interactions (the results for SDI and P + Q.Q interactions are given in Appendix B; here $V_{\alpha\beta}^{[0][2]}$ is negligible by definition). It is seen from the figures that $V_{\alpha\beta}^{[0][2]}$ fluctuates around zero and most strikingly $V_{\alpha\beta}^{[0][2]}$ are seen to follow closely $V_{\alpha\beta}$. Thus one can conclude that $V_{\alpha\beta}^{[0][2]}$ are essentially zero (hence $V^{[0][2]}$ can be neglected) in general. In order to quantify the above observations, norms (3.12, 3.14) of various parts of $h + V^{[0]}$ are calculated and the results are given in Table 3.6. It is seen from the last column of Table 3.6 that irrespective of the space and the interaction, in all the cases considered, the error in the norm of the operator $(h^{[0][1]} + V^{[0][1]} + V^{[0][2]})$ is negligible 2%

Table 3.3 The unitary orbit α, the number of states N_α in the unitary orbit α and the mean single particle energy ϵ_α with respect to each unitary orbit are listed[†].

Space	Interaction	α	N_α	ϵ_α (MeV)
(ds)[a]	CW	1	12	−2.312
	PW	1	12	−2.312
	UNIV-SD	1	12	−1.952
	BONN-J	1	12	1.838
(fp)[b]	MWH2	1	20	−5.604
	FPM13	1	20	−5.699
#1[c]	KBB	1	22	1.675
(ds,fp)[d]	KUO-7	1	20	12.034
		2	12	−2.312
(ds,fp,sdg)[e]	KUO-12	1	12	−2.312
		2	20	9.874
		3	30	21.027
#2[f]	SDI*	1	20	42.663
		2	12	43.100
		3	30	50.038
		4	14	49.910
	P + Q.Q	1	20	42.663
		2	12	43.100
		3	30	50.038
		4	14	49.910
#3[g]	SDI**	1	30	44.694
		2	14	43.555
		3	42	51.070
		4	16	50.362
	P + Q.Q	1	30	44.694
		2	14	43.555
		3	42	51.070
		4	16	50.362

Table 3.3 (cont'd)

#1 $(2p_{3/2}\ 1f_{5/2}\ 2p_{1/2}\ 1g_{9/2})$

#2 $(1g_{7/2}, 2d_{5/2}, 1h_{11/2}, 2d_{3/2}, 3s_{1/2})^{m_p} \oplus (2f_{7/2}, 1h_{9/2}, 1i_{13/2}, 3p_{3/2}, 2f_{5/2}, 3p_{1/2})^{m_n}$

#3 $(1h_{9/2}, 1i_{13/2}, 2f_{7/2}, 2f_{5/2}, 2p_{3/2}, 2p_{1/2})^{m_p}$, $(2g_{9/2}, 1j_{15/2}, 1i_{11/2}, 3d_{5/2}, 2g_{7/2}, 4s_{1/2}, 3d_{3/2})^{m_n}$

a The spherical orbits $(1d_{5/2}, 1d_{3/2}, 2s_{1/2})$, define the unitary orbit $\alpha = 1$ with $s = 0$. The proton and neutron unitary orbits are same.

b The spherical orbits $(1f_{7/2}, 2p_{3/2}, 1f_{5/2}, 2p_{1/2})$ define the unitary orbit $\alpha = 1$ with $s = 0$. The proton and neutron unitary orbits are same.

c The spherical orbits $(2p_{3/2}, 1f_{5/2}, 2p_{1/2}, 1g_{9/2})$ define the unitary orbit $\alpha = 1$ with $s = 0$. The proton and neutron unitary orbits are same.

d The spherical orbits $(1f_{7/2}, 1f_{5/2}, 2p_{3/2}, 2p_{1/2})$ and $(1d_{5/2}, 1d_{3/2}, 2s_{1/2})$ define the unitary orbits $\alpha = 1$ and 2 with $s = 0$ and 1 respectively. The proton and neutron unitary orbits are same.

e The spherical orbits $(1d_{5/2}, 2s_{1/2}, 1d_{3/2})$, $(1f_{7/2}, 2p_{3/2}, 1f_{5/2}, 2p_{1/2})$ and $(1g_{9/2}, 2d_{5/2}, 1g_{7/2}, 3s_{1/2}, 2d_{3/2})$ define the unitary orbits $\alpha = 1$, 2 and 3 with $s = 0$, 1 and 2 respectively. The proton and neutron unitary orbits are same.

f The spherical orbits $(1g_{7/2}, 2d_{5/2}, 2d_{3/2}, 3s_{1/2})$, $(1h_{11/2})$ define $\alpha = 1, 2$ for protons and $(2f_{7/2}, 1h_{9/2}, 3p_{3/2}, 2f_{5/2}, 3p_{1/2})$, $(1i_{13/2})$ define $\alpha = 3,4$ for neutrons. All unitary orbits have $s = 0$.

g The spherical orbits $(1h_{9/2}, 2f_{7/2}, 2f_{5/2}, 2p_{3/2}, 2p_{1/2})$, $(1i_{13/2})$ define $\alpha = 1, 2$ for protons and $(2g_{9/2}, 1i_{11/2}, 3d_{5/2}, 2g_{7/2}, 4s_{1/2}, 3d_{3/2})$, $(1j_{15/2})$ define $\alpha = 3,4$ for neutrons. All unitary orbits have $s = 0$.

* In this case, values are given for $^{168}_{68}Er_{100}$. For other rare-earth nuclei the scale factor $41/A^{1/3}$ should be used.

** In this case, values are given for $^{239}_{92}U_{147}$. For other actinide nuclei the scale factor $41/A^{1/3}$ should be used.

† References for various interactions are given in the text.

Table 3.4 The unitary orbits (α and β) indices, two particle unitary orbit dimensionality $\check{N}_{\alpha\beta}$ and the $V_{\alpha\beta}$ that defines the $V^{[0][0]}$ for several 2-body interactions (pp, nn and pn parts are given separately) in different spaces are tabulated[†].

Space Interaction	α	β	pp		nn		pn	
			$\check{N}_{\alpha\beta}$	$V_{\alpha\beta}$ (MeV)	$\check{N}_{\alpha\beta}$	$V_{\alpha\beta}$ (MeV)	$\check{N}_{\alpha\beta}$	$V_{\alpha\beta}$ (MeV)
(ds)[a]								
CW	1	1	66	−0.144	66	−0.144	144	−1.430
PW	1	1	66	−0.070	66	−0.070	144	−1.407
UNIV-SD*	1	1	66	−0.308	66	−0.308	144	−1.775
BONN-J	1	1	66	−0.347	66	−0.347	144	−1.519
(fp)[b]								
MWH2	1	1	190	−0.005	190	−0.005	400	−0.637
FPM13**	1	1	190	−0.106	190	−0.106	400	−0.720
#1[c]								
KBB	1	1	231	0.016	231	0.016	484	0.444
(ds,fp)[d]								
KUO-7 orbit	1	1	190	−0.439	190	−0.439	400	−1.102
	1	2	240	−0.484	240	−0.484	240	−1.277
	2	2	66	−0.707	66	−0.707	144	−1.778
(ds,fp,sdg)[e]								
KUO-12 orbit	1	1	66	−0.514	66	−0.514	144	−1.307
	1	2	240	−0.353	240	−0.353	240	−0.949
	1	3	360	−0.269	360	−0.269	360	−0.688
	2	2	190	−0.323	190	−0.323	400	−0.821
	2	3	600	−0.245	600	−0.245	600	−0.638
	3	3	435	−0.226	435	−0.226	900	−0.558

Table 3.4 (cont'd)

Space Interaction	α	β	pp		nn		pn	
			$\check{N}_{\alpha\beta}$	$V_{\alpha\beta}$ (MeV)	$\check{N}_{\alpha\beta}$	$V_{\alpha\beta}$ (MeV)	$\check{N}_{\alpha\beta}$	$V_{\alpha\beta}$ (MeV)
$\#2^{J,***}$								
P + Q.Q	1	1	190	0.010	–	–	–	–
	1	2	240	0.000	–	–	–	–
	2	2	66	0.008	–	–	–	–
	3	3	–	–	435	0.016	–	–
	3	4	–	–	420	0.000	–	–
	4	4	–	–	91	0.017	–	–
	1	3	–	–	–	–	600	0.000
	1	4	–	–	–	–	280	0.000
	2	3	–	–	–	–	360	0.000
	2	4	–	–	–	–	168	0.000
$\#3^{g,***}$								
P + Q.Q	1	1	435	0.006	–	–	–	–
	1	2	420	0.006	–	–	–	–
	2	2	91	0.005	–	–	–	–
	3	3	–	–	861	0.009	–	–
	3	4	–	–	672	0.000	–	–
	4	4	–	–	120	0.011	–	–
	1	3	–	–	–	–	1200	0.000
	1	4	–	–	–	–	480	0.000
	2	3	–	–	–	–	588	0.000
	2	4	–	–	–	–	224	0.000

* The quantities are to be multiplied by $(18/A)^{0.3}$

** The quantities are to be multiplied by $(42/A)^{0.35}$

*** The strength G_p, G_n, G^Q_{pp}, G^Q_{nn}, G^Q_{pn} define the P + Q.Q interaction are given in the text. $V_{\alpha\beta}$ for pn part of the interaction is zero (see Appendix B).

† See footnote of Table 3.3 for other details.

For SDI, analytical expressions for $V_{\alpha\beta}$ are available (see Appendix B).

Table 3.5 The unitary one-body part $\epsilon_\alpha^{[1]}$ of NIP hamiltonian h and the renormalized single particle energies $\xi_\alpha^{[1]}([\mathbf{m}])$ (defined by (2.58)), for protons and neutrons, that depend on unitary configurations are compared for each spherical orbit α in different spaces for various interactions. The corresponding pn unitary orbit configurations $[\mathbf{m}_p, \mathbf{m}_n]$ are also given[†].

Space $[\mathbf{m}_p]$ $[\mathbf{m}_n]$	Interaction	α	$\epsilon_\alpha^{[1]}$ (MeV)	$\xi_{\alpha;p}^{[1]}$ (MeV)	$\xi_{\alpha;n}^{[1]}$ (MeV)
$(\mathbf{ds})^a$	UNIV-SD	1	−1.996	−2.458	−2.458
[4]		2	3.599	3.810	3.810
[4]		3	−1.211	−0.246	−0.246
[6]		1	−1.996	−2.691	−2.691
[6]		2	3.599	3.991	3.991
		3	−1.211	0.249	0.249
[6]	BONN-J	1	−1.838	−2.730	−2.730
[6]		2	3.242	4.425	4.425
		3	−0.968	−0.660	−0.660
$(\mathbf{fp})^b$	MWH2	1	3.740	4.298	4.298
[10]		2	−2.760	−3.016	−3.016
[10]		3	−0.660	−0.950	−0.950
		4	1.140	1.072	1.072
	FPM13	1	−2.665	−2.821	−2.821
[2]		2	−0.634	−0.499	−0.499
[2]		3	3.545	3.642	3.642
		4	1.292	1.620	1.620
		1	−2.665	−3.317	−3.317
[8]		2	−0.634	−0.002	−0.002
[8]		3	3.545	3.938	3.938
		4	1.292	1.458	1.458
$\#1^c$	KBB	1	−1.675	−1.845	−1.845
[8]		2	−0.895	−2.574	−2.574
[8]		3	−0.595	−0.775	−0.775
		4	1.325	2.437	2.437

Table 3.5 (cont'd)

Space $[\mathbf{m}_p]$ $[\mathbf{m}_n]$	Interaction	α^*	$\epsilon_\alpha^{[1]}$ (MeV)	$\xi_{\alpha;p}^{[1]}$ (MeV)	$\xi_{\alpha;n}^{[1]}$ (MeV)
(ds,fp)[d]	KUO-7	1	−1.838	−2.039	−2.008
[4 0]		2	3.242	3.460	3.387
[2 2]		3	−0.968	−0.803	−0.750
		4	−2.664	−3.231	−3.275
		5	3.526	3.794	3.656
		6	−0.664	−0.310	−0.098
		7	1.366	2.159	2.328
[5 1]		1	−1.838	−2.161	−2.161
[5 1]		2	3.242	3.575	3.575
		3	−0.968	−0.666	−0.666
		4	−2.664	−3.629	−3.629
		5	3.526	3.856	3.856
		6	−0.664	0.074	0.074
		7	1.366	2.803	2.803
(ds,fp,sdg)[e]	KUO-12	1	−1.838	−2.060	−2.060
		2	−0.968	−0.645	−0.645
		3	3.242	3.413	3.413
		4	−2.664	−3.341	−3.341
		5	−0.664	0.048	0.048
[6 0 0]		6	3.526	3.596	3.596
[6 0 0]		7	1.366	2.480	2.480
		8	−3.247	−3.824	−3.824
		9	1.253	1.384	1.384
		10	0.753	1.393	1.393
		11	2.753	2.265	2.265
		12	3.353	3.564	3.564

Table 3.5 (cont'd)

Space $[\mathbf{m}_p]$ $[\mathbf{m}_n]$	Interaction	α^*	$\epsilon_\alpha^{[1]}$ (MeV)	$\xi_{\alpha;p}^{[1]}$ (MeV)	$\xi_{\alpha;n}^{[1]}$ (MeV)
	KUO-12	1	−1.838	−2.407	−2.437
		2	−0.968	−0.102	−0.075
		3	3.242	3.662	3.693
		4	−2.664	−4.296	−4.304
		5	−0.664	1.000	0.875
[12 4 2]		6	3.526	3.717	3.832
[12 10 0]		7	1.366	4.032	3.970
		8	−3.247	−5.100	−5.007
		9	1.253	1.963	1.685
		10	0.753	1.860	2.110
		11	2.753	3.014	2.545
		12	3.353	4.580	4.498

* For UNIV-SD, BONN-J interactions α = 1, 2 and 3 correspond to $1d_{5/2}$, $1d_{3/2}$ and $2s_{1/2}$ spherical orbits respectively.

For MWH2 interaction α = 1, 2, 3 and 4 correspond to $1f_{5/2}$, $1f_{7/2}$, $2p_{3/2}$ and $2p_{1/2}$ spherical orbits respectively; for FPM13 interaction α = 1, 2, 3 and 4 correspond to $1f_{7/2}$, $2p_{3/2}$, $1f_{5/2}$ and $2p_{1/2}$ spherical orbits respectively.

For KBB interaction α = 1, 2, 3 and 4 correspond to $2p_{3/2}$, $1f_{5/2}$, $2p_{1/2}$ and $1g_{9/2}$ spherical orbits respectively.

For KUO-7 orbit interaction α = 1, 2, 3, 4, 5, 6 and 7 correspond to $1f_{7/2}$, $1f_{5/2}$, $2p_{3/2}$, $2p_{1/2}$, $1d_{5/2}$, $1d_{3/2}$ and $2s_{1/2}$, spherical orbits respectively.

For KUO-12 orbit interaction α = 1, 2, 3, 4, 5, 6, 7, 8, 9, 10, 11 and 12 correspond to $1d_{5/2}$, $2s_{1/2}$, $1d_{3/2}$, $1f_{7/2}$, $2p_{3/2}$, $1f_{5/2}$, $2p_{1/2}$, $1g_{9/2}$, $2d_{5/2}$, $1g_{7/2}$, $3s_{1/2}$ and $2d_{3/2}$ spherical orbits respectively.

† For other symbols in the table, see footnotes of Table 3.3.

Results for rare-earth and actinide nuclei with SDI and P + Q.Q interactions are not shown as for SDI, the SPE renormalization is zero, i.e. $\xi_\alpha^{[1]} = \epsilon_\alpha^{[1]}$ and the renormalization is negligibly small for P + Q.Q interaction.

Figure 3.2

(a) $V_{\alpha\beta}$ matrix elements of $V^{[0]}$ and $V^{[0][2]}$ vs $(\alpha\beta)$ for various ds-shell interactions. Results are shown for pp and pn parts of the interactions (note that pp and nn parts are identical). The definition of the index α (and β) is given in the footnote to Table 3.5. The $V_{\alpha\beta}$ and $V_{\alpha\beta}^{[0][2]}$ are in MeV units. Text and the footnotes to Tables 3.3, 3.5 give further details.

(b) $V_{\alpha\beta}$ matrix elements of $V^{[0]}$ and $V^{[0][2]}$ vs $(\alpha\beta)$ for various fp-shell interactions. Results are shown for pp and pn parts of the interactions (note that pp and nn parts are identical). The definition of the index α (and β) is given in the footnote to Table 3.5. The $V_{\alpha\beta}$ and $V_{\alpha\beta}^{[0][2]}$ are in MeV units. Text and the footnotes to Tables 3.3, 3.5 give further details.

(c) $V_{\alpha\beta}$ matrix elements of $V^{[0]}$ and $V^{[0][2]}$ vs β for various α values for KUO-10 orbit interaction in ($1f_{7/2}$, $1f_{5/2}$, $2p_{3/2}$, $2p_{1/2}$, $1d_{5/2}$, $1d_{3/2}$, $2s_{1/2}$, $1p_{3/2}$, $1p_{1/2}$, $1s_{1/2}$) space with spherical orbit indices α = 1,2,...., 10 respectively for protons (and neutrons). Results are shown for pp and pn parts of the interactions (note that pp and nn parts are identical). The $V_{\alpha\beta}$ and $V_{\alpha\beta}^{[0][2]}$ are in MeV units. See text and footnote to Tables 3.3, 3.5 for further details. The orbits ($1f_{7/2}$, $1f_{5/2}$, $2p_{3/2}$, $2p_{1/2}$), ($1d_{5/2}$, $1d_{3/2}$, $2s_{1/2}$), ($1p_{3/2}$, $1p_{1/2}$) and ($1s_{1/2}$) define the unitary orbits $\boldsymbol{\alpha}$ = 1, 2, 3 and 4 for protons (and neutrons). The $V_{\alpha\beta}$ and $V_{\alpha\beta}^{[0][2]}$ for the KUO - 7 orbit interactions are same as that of KUO - 10 orbit interaction with $\alpha, \beta \in 1f_{7/2}$, $1f_{5/2}$, $2p_{3/2}$, $2p_{1/2}$, $1d_{5/2}$, $1d_{3/2}$, $2s_{1/2}$ and therefore they can be read off from the figure.

ds–SHELL INTERACTIONS

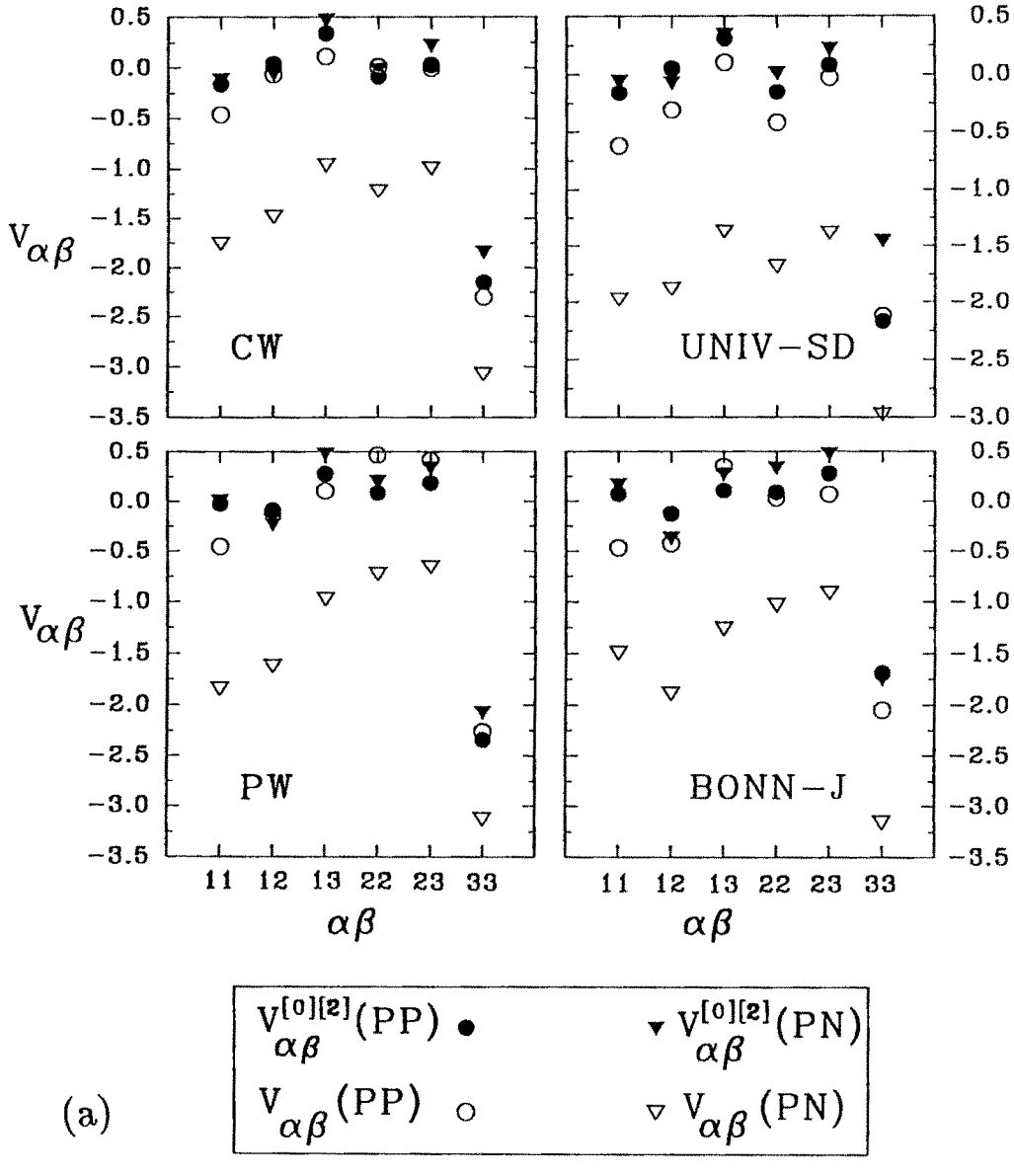

(a)

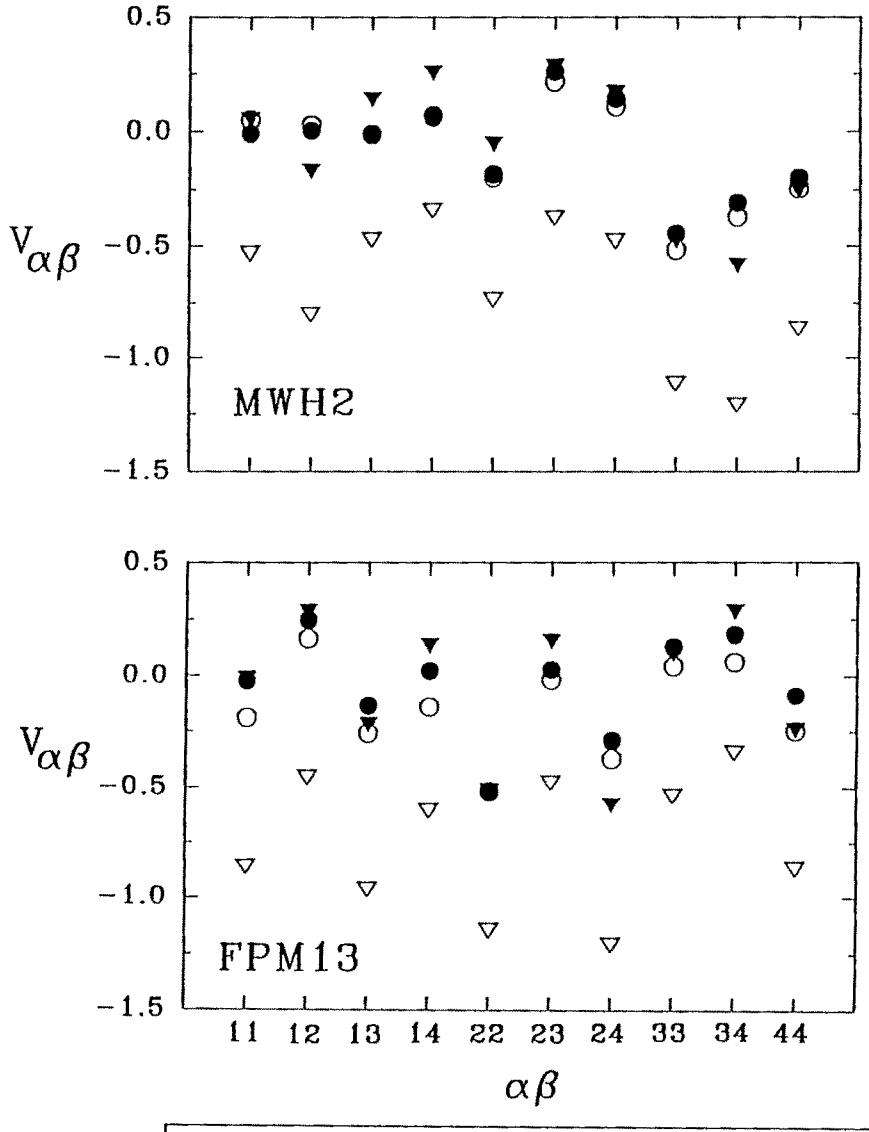

(b)

$V^{[0][2]}_{\alpha\beta}$(PP) ● ▼ $V^{[0][2]}_{\alpha\beta}$(PN)

$V_{\alpha\beta}$(PP) ○ ▽ $V_{\alpha\beta}$(PN)

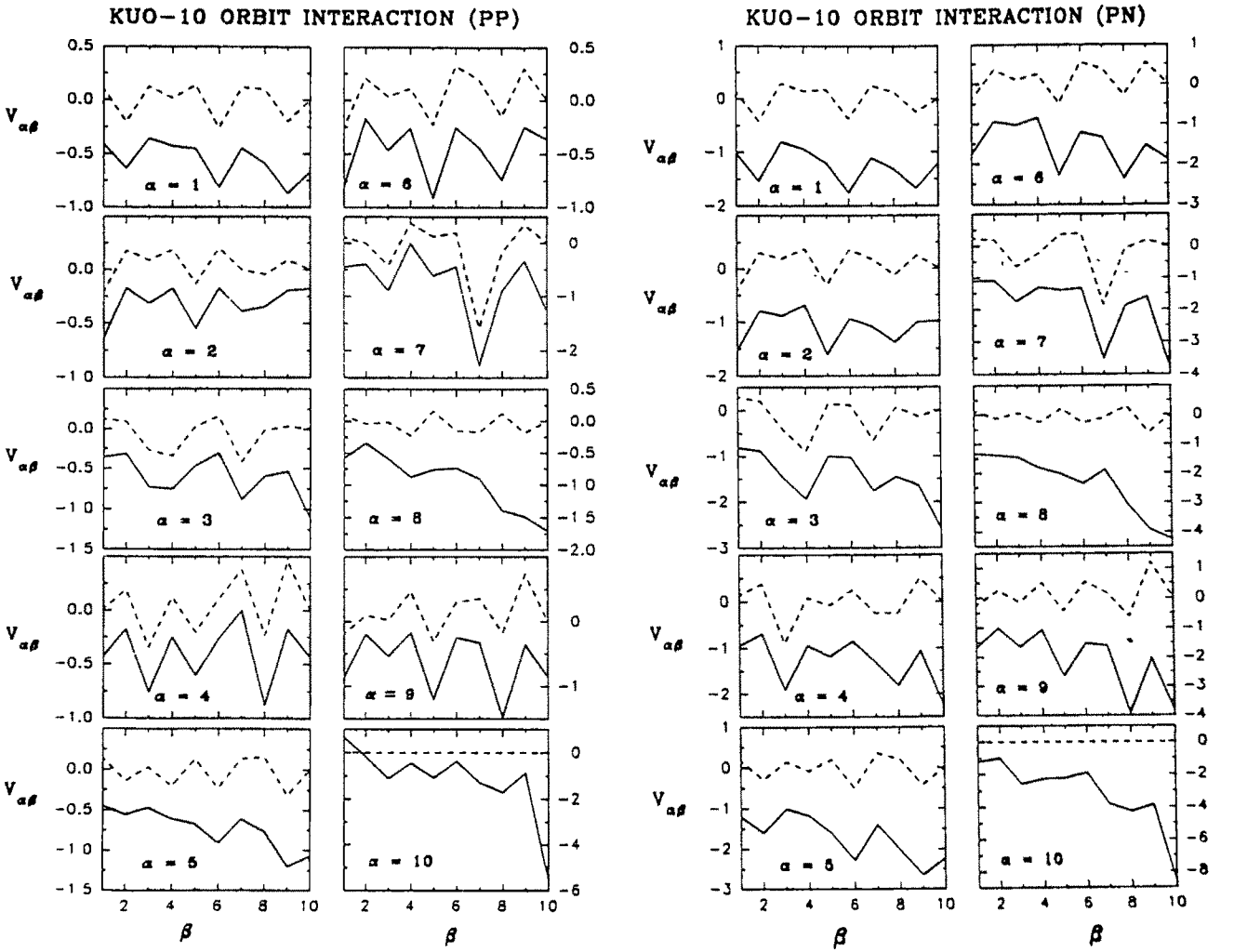
KUO−10 ORBIT INTERACTION (PP)
KUO−10 ORBIT INTERACTION (PN)
$V_{\alpha\beta}$
α = 1
α = 2
α = 3
α = 4
α = 5
α = 6
α = 7
α = 8
α = 9
α = 10
β

(c)

Table 3.6 Norms (in MeV) of various tensor parts of $h + V^{[0]}$. Last column gives the percentage error in the norm of $H^{[0][1]} + V^{[0][2]}$ when $V^{[0][2]}$ is put to zero †.

Space	interaction	(m_p, m_n, S)	$\|h^{[0][1]}\|$	$\|V^{[0][1]}\|$	$\|H^{[0][1]}\|$	$\|V^{[0][2]}\|$	Error
$(ds)^a$	PW	(4,6,0)	5.75	4.55	10.01	1.66	1.37%
		(8,8,0)	5.58	7.33	12.55	1.55	0.77%
	UNIV-SD	(4,6,0)	6.36	1.65	7.16	1.16	1.32%
		(8,8,0)	6.17	2.51	7.50	1.02	0.93%
	BONN-J	(4,4,0)	5.58	1.42	6.94	1.43	2.13%
		(6,8,0)	5.75	2.76	8.41	1.53	1.65%
	P + Q.Q	(4,4,0)	5.58	0.58	5.50	0.43	0.30%
		(4,6,0)	5.75	0.75	5.66	0.41	0.26%
$(fp)^b$	MWH2	(6,6,0)	8.12	0.63	8.72	1.24	1.01%
		(10,10,0)	8.86	1.20	9.99	1.49	1.11%
	FPM13	(6,6,0)	7.79	1.23	8.74	1.21	0.96%
		(10,10,0)	8.50	2.18	10.21	1.38	0.92%
$\#1^c$	KBB	(4,6,0)	3.53	1.97	5.23	0.89	1.44%
		(8,8,0)	4.08	3.78	7.43	1.21	1.32%
$(ds, fp)^d$	KUO-7	(4,4,0)	5.58	0.56	6.04	1.66	3.78%
		(4,4,2)	6.27	0.85	6.84	1.57	2.64%
		(6,6,0)	5.92	0.94	6.72	1.88	3.91%
		(6,6,2)	6.86	1.45	7.91	2.00	3.21%
$(ds, fp,$ $sdg)^e$	KUO-12	(6,6,0)	5.92	0.58	6.31	1.39	0.69%
		(6,6,1)	6.43	0.82	6.91	1.43	2.15%
		(6,6,2)	6.81	0.93	7.33	1.46	1.99%
		(6,6,3)	7.10	0.98	7.65	1.48	1.87%
		(6,6,4)	7.33	1.00	7.89	1.48	1.76%
		(18,22,0)	8.14	4.75	11.46	1.35	0.69%
		(18,22,1)	8.49	4.80	11.87	1.43	0.72%
		(18,22,2)	8.81	4.84	12.25	1.51	0.76%
$\#2^f$	SDI	(14,10,0)	4.74	0.00	4.74	0.04	$\sim 0.00\%$
		(22,24,0)	4.94	0.00	4.94	0.04	$\sim 0.00\%$
	P + Q.Q	(14,10,0)	4.74	0.14	4.87	0.09	0.02%
		(24,25,0)	4.80	0.27	5.04	0.09	0.02%
$\#3^g$	SDI	(8,16,0)	6.33	0.00	6.33	0.03	$\sim 0.00\%$
		(10,21,0)	6.77	0.00	6.77	0.03	$\sim 0.00\%$
	P + Q.Q	(8,16,0)	6.33	0.12	6.41	0.08	0.01%
		(13,21,0)	7.00	0.16	7.12	0.09	0.01%

† see footnotes of Table 3.3 and text for details

or less when $V^{[0][2]}$ is dropped; only in the case KUO-7 interaction in (ds, fp) space, the error is $\sim 3\%$.

In conclusion, it is clearly confirmed, by the results shown in Table 3.6, that the $V^{[0][2]}$ part of the interaction can be neglected irrespective of which part of the periodic table one is dealing with, as seen from the results obtained for variety of interactions that span the entire periodic table. Thus the generality of one of the important assumptions made in the level density theory with interactions as given by (3.3), (3.4) is established. Finally it is worth remarking that the negligible renormalization of SPE produced by SDI and P + Q.Q interactions and that the corresponding $V^{[0][2]}$ part is negligible show that these phenomenological interactions built into them one of the important requirements for the applicability of the level density theory with interactions.

3.3 Tests of moment methods for NIP state, spin-cutoff and occupancy densities

In order to test, in large spaces, the moment theory given in Sect. 3.1.4 for NIP state, spin-cutoff and occupancy densities and their S-decompositions, a case of twelve protons ($m_p = 12$) and twelve neutrons ($m_n = 12$) in sixteen spherical orbits is considered with $S\hbar\omega = 0$ to $4\hbar\omega$ excitations. The s.p. orbits are ($\alpha = 1-16$) $1s_{1/2}$, $1p_{3/2}$, $1p_{1/2}$, $1d_{5/2}$, $2s_{1/2}$, $1d_{3/2}$, $1f_{7/2}$, $2p_{3/2}$, $1f_{5/2}$, $2p_{1/2}$, $1g_{9/2}$, $2d_{5/2}$, $1g_{7/2}$, $3s_{1/2}$, $2d_{1/2}$, $1h_{11/2}$ and the corresponding SPE (in MeV) are 0.0, 8.076, 12.206, 16.388, 20.596, 21.851, 24.752, 29.431, 31.208, 32.201, 33.116, 38.213, 40.383, 41.297, 42.238, 41.454 respectively. The SPE follow from Seeger energies for neutrons; Ref. [Hi-69] gives the Seeger energies. The spherical orbits are divided into eight unitary orbits (α = 1-8) and they are

$[1s_{1/2}]$, $[1p_{3/2}, 1p_{1/2}]$, $[1d_{5/2}, 2s_{1/2}, 1d_{3/2}]$, $[1f_{7/2}]$, $[2p_{3/2}, 1f_{5/2}, 2p_{1/2}]$, $[1g_{9/2}]$, $[2d_{5/2}, 1g_{7/2}, 3s_{1/2}, 2d_{3/2}]$, and $[1h_{11/2}]$. The corresponding s values and parities ($s(\pi)$) are 0(+), 1(−), 2(+), 3(−), 3(−), 4(+), 4(+) and 5(−) respectively (in the above choice, parity is uniquely defined for a given s and therefore parity is dropped in the remaining part of this section; in principle one can take s = 4 for $1h_{11/2}$ orbit but then one has to decompose the space according to s and π). Results for state, spin-cutoff and occupancy densities are given in Figs. 3.3a - 3.3f. In the figures the exact results are obtained by direct counting method (i.e. by using spherical configurations ($\mathbf{m}_p$, $\mathbf{m}_n$)). Results shown in Figs. 3.3a - 3.3f are first reported in [Ko-92a].

Comparison with direct counting results

The state densities and their decompositions are well described by the moment methods as shown in Fig. 3.3a and they confirm that the earlier results by Smith [Sm-87; also Ko-91] for identical particles (Smith dealt with 36 neutrons in 31 spherical orbits) extend to the realistic case with protons and neutrons. As can be seen from Fig. 3.3a, the essentially Gaussian densities for a given S add up to give exponential form (as in Bethe's Fermi gas theory; Eq. (C.1) of Appendix C ahead) for the state densities and this has its origin in the fact that at the energy where a given S-density peaks, the density for a higher S (which is displaced with respect to the lower S density) dominates and this continues. It should be mentioned that calculations for pn systems without S-decompositions (therefore they do not tell much about origin of the exponential form of the state density) are given in [Ha-80]. Fig. 3.3b shows that moment methods give good description of spin-cutoff densities and their S-decompositions. The quality of agreement is similar to that of state

Figure 3.3

(a) Comparison of exact counting results with moment theory for state densities $I(E)$ and the corresponding S-decompositions $I^{h,S}(E)$. The exact results are averaged over 2 MeV bins. $I(E)$ is in MeV^{-1} units and shown in the figure is $\ell og(I(E))$ vs E. Text gives details regarding special orbits, s values, unitary orbits etc.

(b) Same as Fig. 3.3a but for J_Z^2 - densities $I^h_{J_Z^2}(E)$ and $I^{h,S}_{J_Z^2}(E)$.

(c) Same as Fig. 3.3a but for n_α - densities $I^h_{n_\alpha}(E)$ and $I^{h,S}_{n_\alpha}(E)$; $\alpha = 1d_{5/2}$ proton orbit. The results are same for $1d_{5/2}$ neutron orbit.

(d) Same as Fig. 3.3c but for $\alpha = 1f_{7/2}$ proton orbit.

(e) Comparison of moment theory results with exact results (averaged over 2 MeV bins) for state densities $(I(E))$, spin-cutoff factors $(\langle J_Z^2\rangle^E)$ and occuaption number $\langle n_\alpha\rangle^E$. The $\langle n_\alpha\rangle^E$ results are given for proton orbits $1d_{5/2}$ and $1f_{7/2}$. The results are same for corresponding neutron orbits. Shown in the figure are also the comparison of moment method results with fermi gas forms (see text) for $I(E)$ and $\langle J_Z^2\rangle^E$.

(f) Comparison of fractional occupancies (for protons) $n_{\epsilon_\alpha}(E)$ calculated using moment theory with Fermi-Dirac form (3.16) for $E = 5$, 21 and 41 MeV. The SPE ϵ_α are given in the text for the orbits α used in the calculations. The results are same for neutrons.

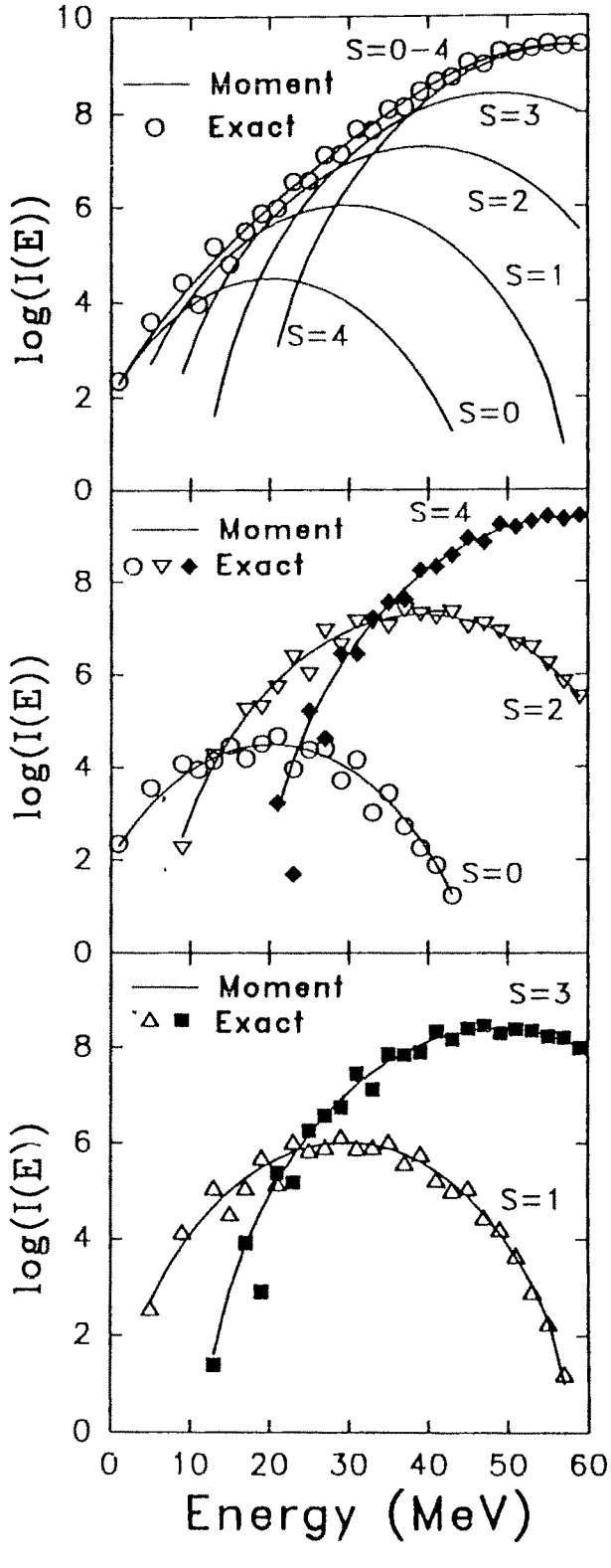
log(I(E))
Moment
Exact
S=0-4
S=3
S=2
S=1
S=4
S=0
S=4
S=2
S=0
S=3
S=1
0
2
4
6
8
10
0
10
20
30
40
50
60
Energy (MeV)

(a)

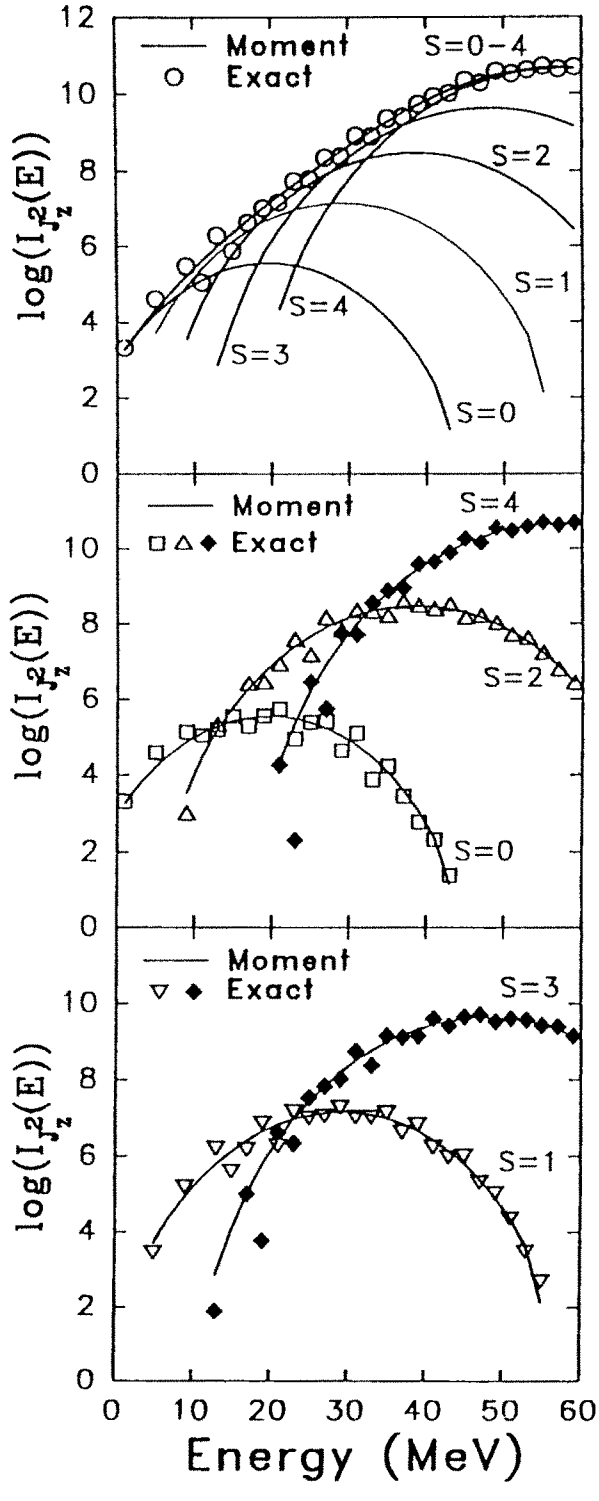
Moment
Exact
S=0-4
S=2
S=1
S=4
S=3
S=0
Moment
Exact
S=4
S=2
S=0
Moment
Exact
S=3
S=1
log(I_Jz^2(E))
Energy (MeV)

(b)

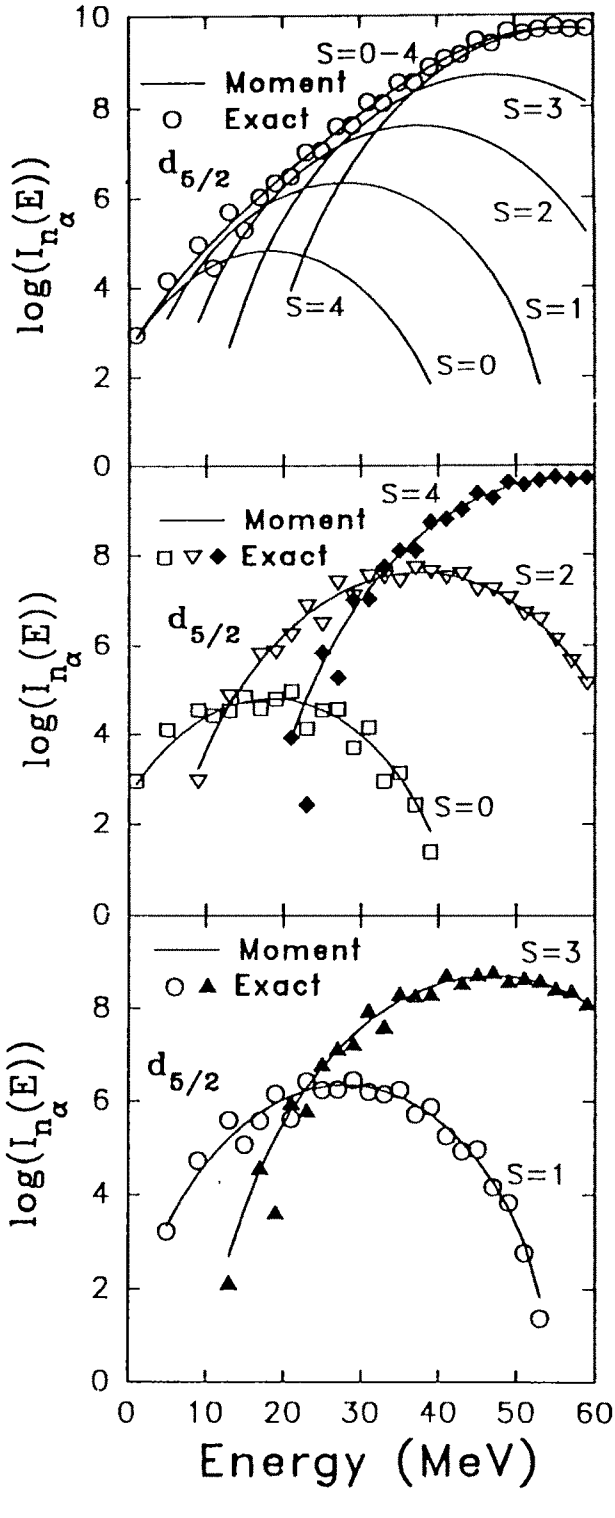
S=0-4
Moment
Exact
$d_{5/2}$
S=3
S=2
S=1
S=0
S=4
$\log(I_{n_\alpha}(E))$
Moment
Exact
$d_{5/2}$
S=4
S=2
S=0
Moment
Exact
$d_{5/2}$
S=3
S=1
0 10 20 30 40 50 60
Energy (MeV)

(c)

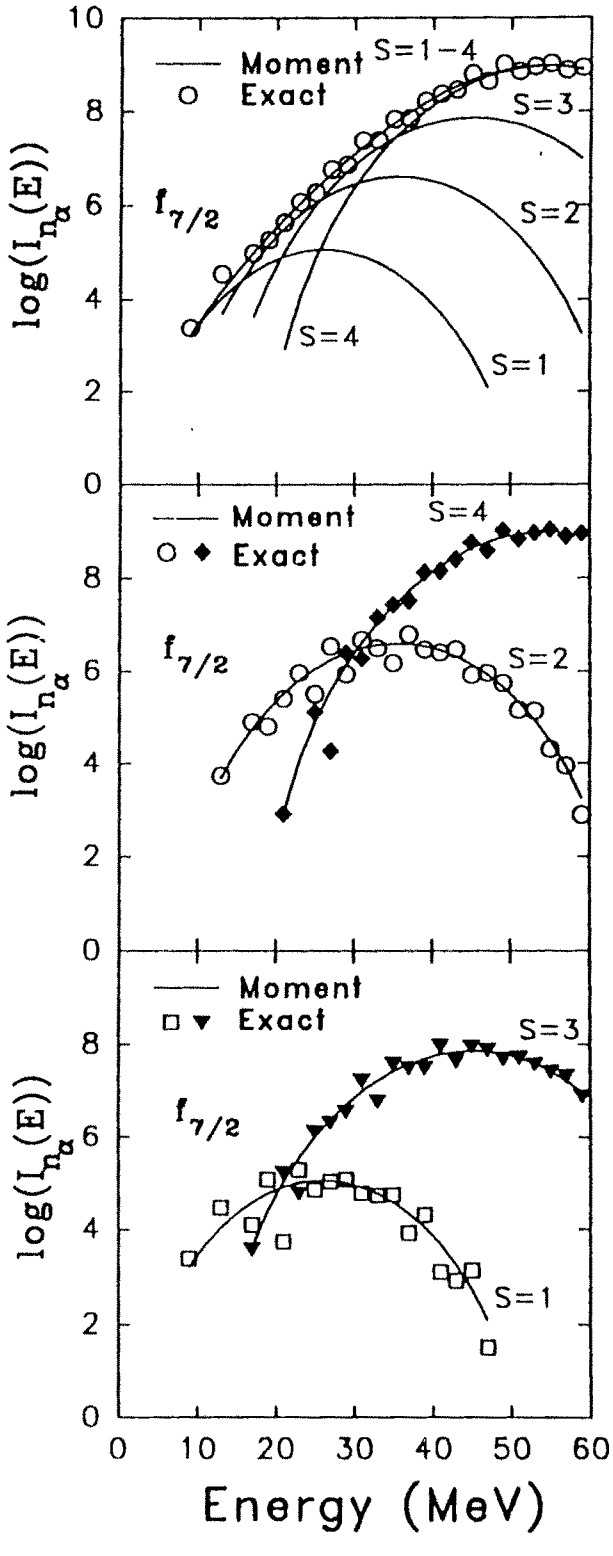

(d)

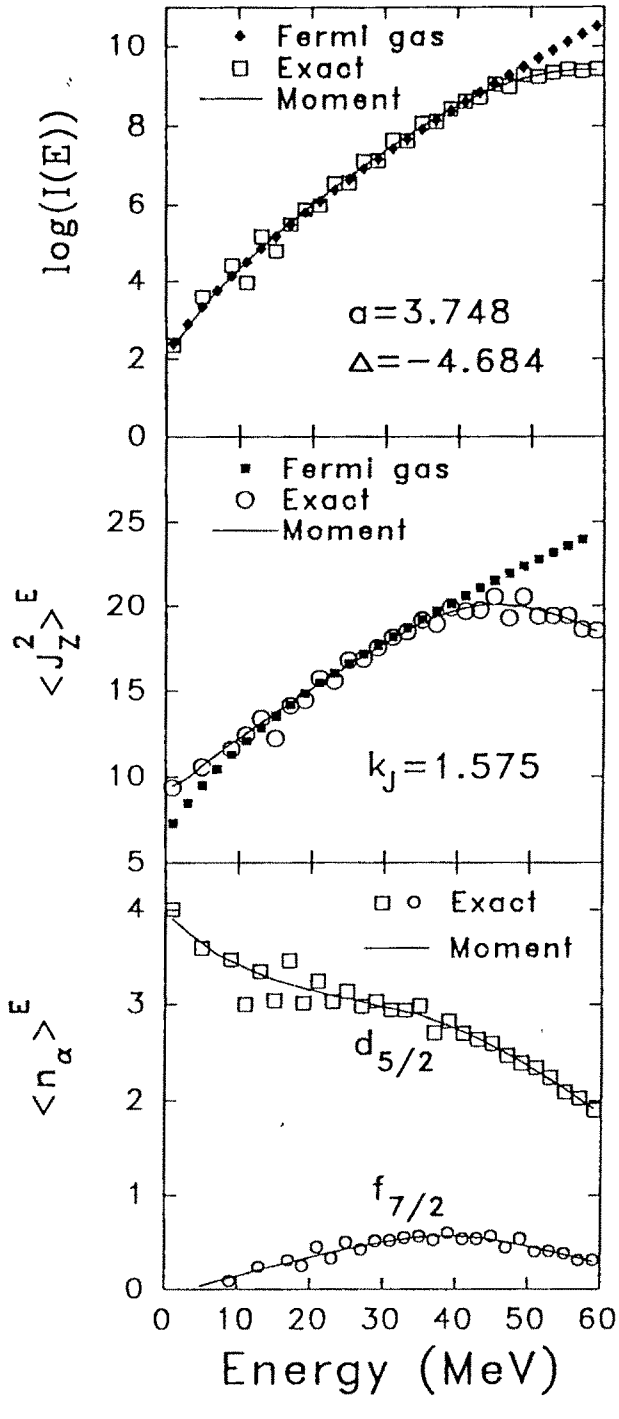
Fermi gas
Exact
Moment
log(I(E))
a=3.748
Δ=−4.684
Fermi gas
Exact
Moment
$\langle J_z^2 \rangle^E$
k_J=1.575
Exact
Moment
$\langle n_\alpha \rangle^E$
$d_{5/2}$
$f_{7/2}$
Energy (MeV)

(e)

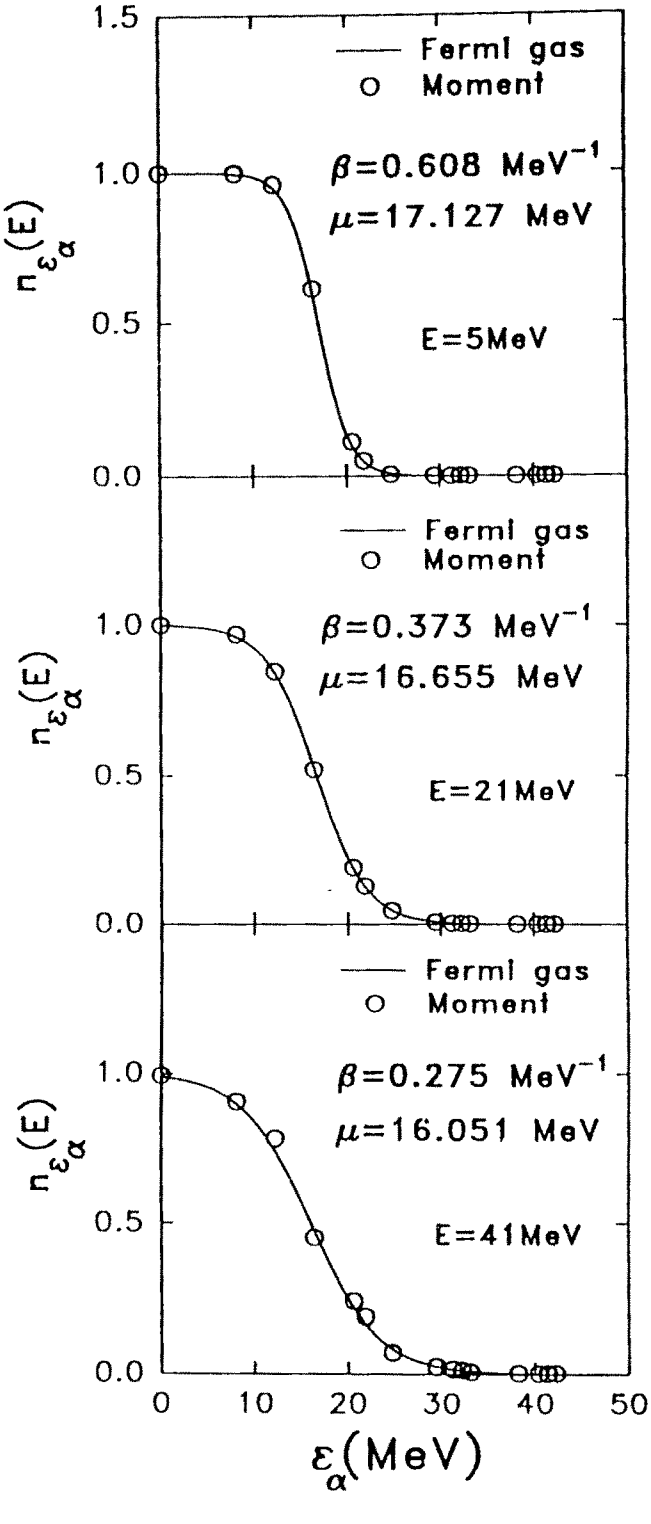
Fermi gas
Moment
β=0.608 MeV⁻¹
μ=17.127 MeV
E=5MeV
Fermi gas
Moment
β=0.373 MeV⁻¹
μ=16.655 MeV
E=21MeV
Fermi gas
Moment
β=0.275 MeV⁻¹
μ=16.051 MeV
E=41MeV
n_εα(E)
ε_α(MeV)
0.0
0.5
1.0
1.5
0
10
20
30
40
50

(f)

densities. Here once again the total spin-cutoff densities have exponential form. The centroids ϵ (in MeV) of $I^{h,S}_{J^2_Z}(E)$ densities are 264.2, 273.81, 283.35, 292.85 and 302.32 for $S = 0, 1, 2, 3$ and 4 respectively. Thus each state density is shifted by $\simeq 10\ MeV$ from its neighbor and this explains the exponential behavior of J^2_Z - density as seen in Fig. 3.3b. The average (σ (in MeV), γ_1, γ_2) values for the unitary orbit configurations that belong to a given S are (5.86, −0.01, −0.13), (6.06, −0.01, −0.13), (6.22, −0.01, −0.12), (6.35, −0.01, −0.12) and (6.46, −0.02, −0.12) for $S = 0, 1, 2, 3$ and 4 respectively. For the state densities $I^S(E)$, $\gamma_1 \simeq -0.01$, $\gamma_2 \simeq -0.13$ while (ϵ, σ) (in MeV) take the values (264.71, 6.17), (274.17, 6.31), (283.63, 6.43), (293.08, 6.54) and (302.52, 6.62) for $S = 0, 1, 2, 3$ and 4 respectively. The widths σ for $I^{h,S}_{J^2_Z}(E)$ are consistently smaller than the widths for $I^{h,S}(E)$ and same is true for centroids. The (γ_1, γ_2) values given above confirm the action of CLT for NIP state and spin-cutoff densities. The quality of agreements seen from J^2_Z-density extends to occupancy densities and in Figs. 3.3c, 3.3d the results for $1d_{5/2}$ and $1f_{7/2}$ densities are shown. As an example, the centroids (in MeV) of $I^{h,S}_{n_\alpha}(E)$ for $1d_{5/2}$ orbit are 262.88, 272.34, 281.80, 291.25 and 300.68 for $S = 0, 1, 2, 3$ and 4 respectively. The centroids shift ($\simeq 10\ MeV$) with respect to S explains the exponential increase in $I^{h,S}_{n_\alpha}(E)$ with E. The average (σ (in MeV), γ_1, γ_2) values for the unitary orbit configurations that belong to a given S (for $d_{5/2}$ occupancy density) are (5.88, 0.0, −0.16), (6.03, −0.01, −0.16), (6.16, −0.02, −0.16), (6.27, −0.03, −0.15) and (6.36, −0.03, −0.15) for $S = 0, 1, 2, 3$ and 4 respectively. In order to further test the results for J^2_Z and n_α - densities, spin-cutoff factors and occupation numbers are calculated as ratios of densities,

$$\sigma^2_J(E) = \langle J^2_Z \rangle^E = I^h_{J^2_Z}(E)/I^h(E)$$

$$\langle n_\alpha \rangle^E = I^h_{n_\alpha}(E)/I^h(E) \tag{3.15}$$

and the corresponding results are shown in Fig. 3.3e. One sees that moment methods describe $\langle J_Z^2 \rangle^E$ and $\langle n_\alpha \rangle^E$ in large spaces very well. The variation in $\langle J_Z^2 \rangle^E$ and $\langle n_\alpha \rangle^E$ with E can be understood by replacing the fixed-S densities by Gaussians and using the fact the (ϵ, σ) values for $I^{h,S}(E)$ densities are smaller (the deviations are larger for $1d_{5/2}$ densities) than the corresponding values for $I^{h,S}_K(E)$ densities; $K = J_Z^2$ or n_α with $\alpha = 1d_{5/2}$. Calculations for $\langle J_Z^2 \rangle^E$ and $\langle n_\alpha \rangle^E$ for 'nucleons' are reported in [Ko-91] while in the present exercise more realistic pn system is dealt with. It should be added that calculations for different (m_p, m_n) sets are carried out and also with different SPE for protons and neutrons and the results are found to be similar to the results shown in Figs. 3.3a - 3.3e.

Comparison with Fermi gas forms

It is important to understand how close the moment method results are to the NIP forms as the later forms are widely used in literature in analyzing data (Appendix C gives a summary of various Fermi gas forms). Recently comparison of Fermi gas forms with exact results are given by Grimes [Gr-88] and they are not of much use as the Fermi forms are not compared with a theory that can be extended easily to the interacting particle case. The same is true with the recursive method for calculating NIP state densities and spin-cutoff factors proposed by Jacquemin and Kataria [Ja-86] and the Monte Carlo method proposed by Cerf [Ce-94]. For state densities of pn systems, the back-shifted Fermi gas form [Hu-72; Eq. (C.1)] is given by $I(E) = (\sqrt{\pi}/12) exp\{(2\sqrt{a(E-\Delta)})/(a^{1/4}(E-\Delta)^{5/4})\}$. In Fig. 3.3e, the fit of the back shifted Fermi gas form with the moment method results is shown

and the deduced value of the level density parameter "a" and the back shifting energy "Δ" are $a = 3.75\ MeV^{-1}$ and $\Delta = -4.68\ MeV$. The Fermi form fits very well upto 45 MeV and beyond that one has to enlarge the single particle space to get good agreements. As it is well known in the Fermi gas theory [Hu-72, Gi-65; Appendix C] the spin-cutoff factors take the form $\sigma_J^2(E) = \langle J_Z^2 \rangle^E = k_J \sqrt{a(E-\Delta)}$ where k_J is taken to be a free parameter ($k_J \propto A^{2/3}$). With the (a, Δ) values determined from the fit to state densities, the calculated $\langle J_Z^2 \rangle^E$ values are fitted to the above form and the results are shown in Fig. 3.3e. The value of k_J is determined to be 1.58. One sees that the Fermi gas form shows departures at lower energies ($E < 10MeV$), as well as at higher energies ($E > 40MeV$). Thus the Fermi gas form cannot be used at lower energies and the discrepancy at higher energies is due to the truncation of the single particle space to sixteen orbits. The parameters (a, Δ, k_J) obtained above are somewhat larger than the values commonly used for real nuclei, i.e. $a \simeq A/8$ to $A/10\ MeV^{-1}$, $|\Delta| \simeq 2\ MeV$ and $k_J \simeq 0.1A^{2/3}$.

From the calculated occupation numbers it is possible to deduce [Sm-87] thermodynamic temperature ($\beta(E)$) and chemical potential ($\mu(E)$) by fitting the fractional occupancies $n_{\epsilon_\alpha}(E)$ to the Fermi-Dirac form,

$$n_{\epsilon_\alpha}(E) = \frac{< n_\alpha >^E}{(2j_\alpha + 1)} = \frac{1}{1 + exp[\beta(E)\{\epsilon - \mu(E)\}]} \tag{3.16}$$

At various energies E, the calculated occupation numbers $\langle n_\alpha \rangle^E$ for the spherical orbits α (with SPE ϵ_α) are fitted to (3.16) and the inverse temperature β and the chemical potential μ are deduced and the results are shown in Fig. 3.3f for $E = 5\ MeV$, 21 MeV and 41 MeV. One sees that occupancies have excellent agreement with Fermi-Dirac form (3.16). With increase in energy as normally one expects, the chemical potential decreases and temperature (β^{-1})

increases; $(\beta(E),\ \mu(E))$ are (in MeV^{-1}, MeV) (0.61, 17.13), (0.37, 16.66) and (0.28, 16.05) for $E = 5$, 21 and 41 MeV respectively. The calculated $(\beta(E),\ \mu(E))$ values are seen to follow closely the approximate Fermi gas expressions $\beta(E) = A/\sqrt{E}$ and $\mu(E)\beta(E) = A' + B'\sqrt{E}$; A, A' and B' are free parameters [2]. Thus it is seen that occupation numbers yield values for thermodynamic temperature. Obviously its extension to the case with interactions is of immense value (Smith [Sm-87] made some preliminary studies of the same; however he did not give any large scale NIP example). Thus the results given in Figs. 3.3a - 3.3f conclusively establish that one has a good theory in moment methods for constructing state, spin-cutoff and occupancy densities, their S-decompositions and for calculating spin-cutoff factors and occupation numbers in large spaces for NIP systems. The agreements shown for S-decompositons of $\langle J_Z^2\rangle^E$ and $\langle n_\alpha\rangle^E$ densities are essential for applying Eqs. (3.3) - (3.6).

3.4 Summary

Two important tests of SAT-LSS are performed in a comprehensive manner and they are described in Sects. 3.2 and 3.3. The test of smallness of $V^{[0][2]}$ demonstrates that one of the conditions for validity of the convolution forms given in (3.3 - 3.6) where the densities are expressed as a convolution of NIP densities (due to **h**) with spreading Gaussians produced by **V**, is well satisfied by nuclear effective interactions. The detailed tests of the moment methods for NIP state, spin-cutoff and occupancy densities clearly show that the moment

[2] $\beta = \frac{\partial}{\partial E}\ell n\, I(E)$ and $\mu_p\beta = \frac{-\partial}{\partial m_p}\ell n(I(E))$, where $m_p = \sum n^p_{\ell_\alpha}(E)$ is proton number. The $\mu_n\beta$ is similarly defined. From the Fermi gas theory $I(E) \sim A_0 e^{B_0\sqrt{E}}$. The form given above for $\mu\beta$ follows by taking $\frac{\partial A_0}{\partial m_p}$ and $\frac{\partial B_0}{\partial m_p}$ to be constants.

methods are well suited, having the desired structures, for constructing the NIP densities which are one of the convolution factors in the IP theory given by (3.3 - 3.6). Further tests of SAT-LSS come from actual data analysis. Towards this end, in the next chapter a systematic analysis of fp-shell level densities and spin-cutoff factors data is carried out.